The effect of temperature on the elastic precursor decay in shock loaded FCC aluminium and BCC iron

Gurrutxaga-Lerma, B.; Shehadeh, M. A.; Balint, D. S.; Dini, D.; Chen, L.; Eakins, D. E.

DOI:
10.1016/j.ijplas.2017.05.001

International Journal of Plasticity 96 (2017) 135–155

Contents lists available at ScienceDirect

International Journal of Plasticity

journal homepage: www.elsevier.com/locate/ijplas

The effect of temperature on the elastic precursor decay in shock loaded FCC aluminium and BCC iron

B. Gurrutxaga-Lerma [a, *], M.A. Shehadeh [b], D.S. Balint [c], D. Dini [c], L. Chen [d], D.E. Eakins [e]

[a] Trinity College Cambridge, Cambridge CB2 1TQ, UK and Department of Engineering, University of Cambridge, Trumpington St, Cambridge CB2 1PZ, UK
[b] Mechanical Engineering Department, American University of Beirut, Beirut 1107 2020, Lebanon
[c] Department of Mechanical Engineering, Imperial College London, Exhibition Rd, London SW7 2AZ, UK
[d] Clarendon Laboratory, University of Oxford, Parks Road, Oxford OX1 3PU, UK
[e] Department of Physics, Imperial College London, Exhibition Rd, London SW7 2AZ, UK

ARTICLE INFO

Article history:
Received 24 March 2017
Received in revised form 9 May 2017
Accepted 12 May 2017
Available online 31 May 2017

Keywords:
Temperature
Dislocations
Shocks
Elastic precursor decay

ABSTRACT

This article offers a comprehensive experimental and theoretical study of the causes of thermal hardening in FCC Al and BCC Fe at high strain rates, with the aim to shed light on important mechanisms governing deformation and failures in materials subjected to shocks and impacts at very high strain rates. Experimental evidence regarding the temperature dependence of the dynamic yield point of FCC Al and BCC Fe shock loaded at 10^7 s^{-1} is provided. The dynamic yield point of Al increases with temperature in the range 125K–795K; for the same loading and temperate range, the dynamic yield point of BCC Fe remains largely insensitive. A Multiscale Discrete Dislocation Plasticity (MDDP) model of both Fe and Al is developed, leading to good agreement with experiments. The importance of the Peierls barrier in Fe is highlighted, showing it is largely responsible for the temperature insensitivity in BCC metals. The relevance of the mobility of edge components in determining the plastic response of both FCC Al and BCC Fe at different temperatures is discussed, which leads to developing a mechanistic explanation of the underlying mechanisms leading to the experimental behaviour using Dynamic Discrete Dislocation Plasticity (D3P). It is shown that the main contributing factor to temperature evolution of the dynamic yield point is not the mobility of dislocations, but the temperature variation of the shear modulus, the decrease of which is correlated to the experimental behaviour observed for both FCC Al and BCC Fe.

1. Introduction

The yield point of most metals loaded with moderate strain rates decreases with increasing temperature (Reed-Hill et al., 2009). This would be brought about by increased mobility of the dislocations in the metal: as temperature increases, dislocations are increasingly able to overcome, through thermal activation, the Peierls barrier that hinders their motion, leading to easier glide. As a result, plastic flow becomes increasingly easy, and hence the yield point drops (Argon, 2008). This applies

* Corresponding author.
E-mail address: bg374@cam.ac.uk (B. Gurrutxaga-Lerma).

http://dx.doi.org/10.1016/j.ijplas.2017.05.001

mostly to metals subjected to very low strain rate and stress levels, low enough as on the one hand, the Peierls barrier cannot be overcome solely by the applied stress; and on the other hand, that increasing the strain rate does not overtake the effect of temperature in facilitating jumping the Peierls barrier (Hirth and Lothe, 1982).

These conditions are not met in shock loading. For one thing, the magnitude of the applied loads easily exceeds both the Peierls barrier and even the ideal lattice strength of the material (Meyers, 1994). For another, the strain rate is high enough that it becomes a dominant factor in activating the motion of dislocations (Armstrong and Walley, 2008; Gurrutxaga-Lerma et al., 2015a). This suggests that dislocation mobility may not be governed by the need to overcome the Peierls barrier anymore, but by the natural lattice resistance to its motion, which manifests itself as a drag force acting on the dislocation (Hirth and Lothe, 1982). In that case, dislocation drag, rather than thermal activation of motion, would dominate the motion of dislocations in shock loading (and therefore plastic flow) (Meyers et al., 2009). This resistance to the motion of dislocations is ultimately caused by phonon scattering and radiation by the dislocation, and by phonon wind effects, and is known to be proportional to temperature: with increasing temperature, the dislocation's drag increases and its motion is consequently hindered (Hirth and Lothe, 1982).

Hence, if yielding is caused by dislocation motion, and if in shock loaded regimes dislocation motion is dominated by phonon drag effects, which in turn are proportional to temperature, one could presume that the plastic yielding of metals should in fact increase with temperature. Experimental observations show that BCC metals such as iron (Zaretsky, 2009; De Rességuier et al., 2012), tantalum (Zaretsky and Kanel, 2014), and vanadium (Zaretsky and Kanel, 2014) do not display this behaviour, and the dynamic yield point either remains unchanged or decreases slightly with temperature. However, FCC metals including aluminium (Zaretsky and Kanel, 2012), silver (Zaretsky and Kanel, 2011) or copper (Zaretsky and Kanel, 2013), and HCP metals like titanium (Kanel et al., 2003) and cobalt (Zaretsky, 2010) do show an increase in the dynamic yield point with temperature.

The extraneous behaviour of BCC metals such as iron contrasts with the behaviour of FCC metals such as aluminium, thereby highlighting the limits of the general assumption that the increase in the yield point with temperature is the result of dislocation-mediated plasticity transiting from a thermally activated regime to a pure drag regime (cf. (Reed-Hill et al., 2009; Meyers, 1994)). The aim of this work is to shed light onto the way temperature may contribute to the attenuation of the dynamic yield point in FCC aluminium and BCC iron. Both materials are chosen because of their characteristic and opposite plastic behaviour under shock loading at different temperatures.

Given that many constitutive models of plastic flow in these regimes rely on physical assumptions for the generation and motion of dislocations, the aim of this work is to provide a comprehensive analysis of the collective motion and dynamic interactions between dislocations. This investigation is aimed at unraveling the mechanisms responsible for the observed yielding of the materials under consideration at different temperatures, and can be employed for the improvement of the said constitutive laws.

In order to provide a comprehensive analysis of this behaviour and the causes leading to it, this work comprises both experimental results, and dislocation dynamics simulations across the length and timescales. Thus, section 2 reports recent experimental results pertaining to FCC aluminium and BCC iron shocked at different temperatures. These experiments show the specific behaviour of the dynamic yield point of Al and Fe at different temperatures and a constant strain rate of $\approx 10^7\ s^{-1}$, confirming that the dynamic yield point of Al increases with temperature, whilst that of Fe remains largely unchanged for the same loading and temperature range. The experimental findings will be compared to and interpreted with the help of mesoscopic models of discrete dislocation dynamics subjected to equivalent loading and temperature. These models will be employed to provide a complete explanation of the causes of the evolution of the dynamic yield point with temperature. To begin with, sections 3 and 4 will present a three dimensional dislocation dynamics approach, *Multiscale Discrete Dislocation Plasticity* (MDDP), with which the inherent differences displayed by FCC Al and BCC Fe upon being shocked at different temperatures will be studied. The MDDP results will confirm that increasing the temperature leads to an increase in the dynamic yield point of FCC Al, whilst the dynamic yield point of BCC Fe remains largely unchanged. The study will highlight the relevance of the mobility of edge components in determining the plastic response of both FCC Al and BCC Fe at different temperatures.

Section 5 concerns the in-depth study of the causes leading to the temperature dependence of the dynamic yield point. Section 4 had shown that the relaxation of the shock front is mostly due to the edge components of the dislocation loops, the screw components lagging behind the front. In fact, Gurrutxaga-Lerma et al. (2015b) showed that within the shock front, plastic yielding and the evolution of the yield point are heavily influenced by the destructive interference of the elastodynamic fields of the dislocations (Gurrutxaga-Lerma et al., 2015b), an effect that cannot be accurately captured with MDDP. Thus, section 5 is devoted to explaining in depth the causes of this behaviour using a *Dynamic Discrete Dislocation Plasticity* (D3P) model where the fields of the dislocations receive an explicit elastodynamic treatment. This will be used to show the effect of temperature on the yield point of shock loaded Al and Fe with increasing temperature, offering a mechanistic interpretation of the role temperature has in the dynamic yielding of metals. Finally, section 6 summarises the main findings of this work.

2. Experimental results

Laser-driven compression experiments were performed at the Trident Laser Facility at Los Alamos National Laboratory. As shown in Fig. 1a, free-standing thin foil samples of aluminium and iron were irradiated with a 527 nm primary drive beam

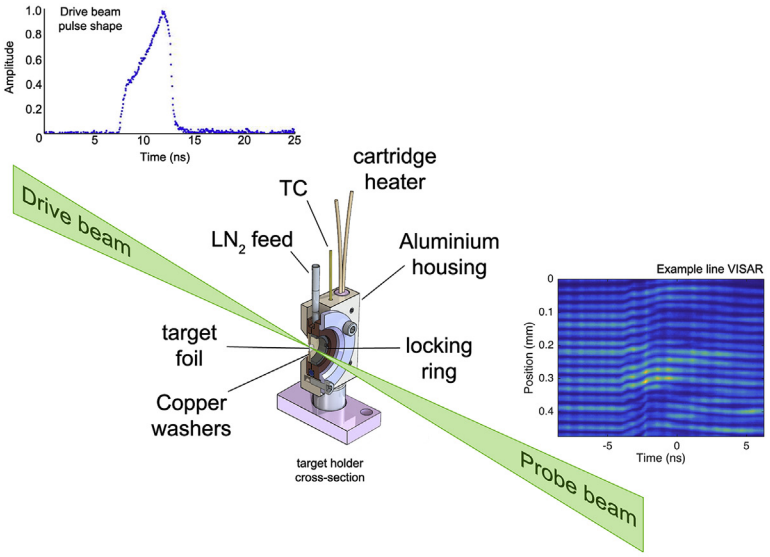

(a) Schematic of the laser-driven shock experiments. The foil samples are clamped within a novel holder which enables heating or cooling to access pre-shock temperatures in the range 80 - 800 K. The samples are irradiated with 100-200 J in a 5 ns shaped pulse (shown at upper left), and diagnosed using line-imaging VISAR.

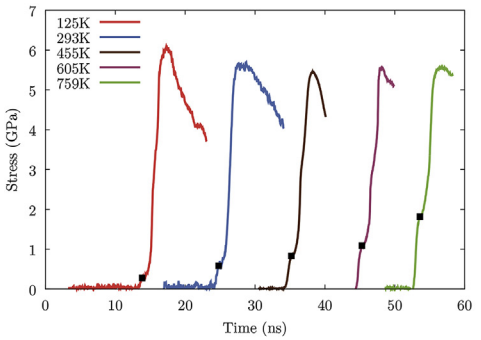

(b) FCC Al.

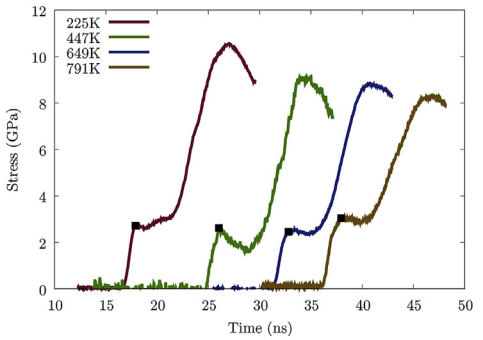

(c) BCC Fe.

Fig. 1. Schematic of the experiments and experimental shock wave profiles for FCC Al and BCC Fe shocked at different temperatures with strain rate of $\approx 10^7$ s^{-1}. The peak of the elastic precursor (the dynamic yield point), marked with a black square, increases with temperature for FCC Al, and remains largely unchanged for BCC Fe. The apparent secondary precursors in FCC Al at 455K and 605K are due to rarefaction waves. Equally, the shocked state is affected by these rarefaction waves.

focused to a 5 mm FWHM near flat-topped spot, delivering pulse energies of 100–200 J over 5 ns for intensities on the order of 10^{11} W/cm^2. A pair of line-imaging velocity interferometers (VISARs) was used to monitor motion of the sample rear surface during arrival of the resulting structured shock wave.

The aluminium and iron samples were acquired as 125 μm foils from Goodfellow, Cambridge Ltd., from which 12 mm diameter discs were prepared. Both materials were supplied in annealed condition, with purities of 99.0% and 99.99% for the aluminium and iron, respectively. EBSD revealed a grain size of 10–50 μm for the aluminium, compared to 40–50 μm for the iron. Both microstructures were comprised of randomly oriented grains.

Prior to dynamic loading, the samples were subjected to a range of temperatures spanning 80–800 K using a novel target holder which enabled control of temperature using a combination of liquid nitrogen and resistive heating. The liquid nitrogen was delivered through 3 mm ID steel tubing in an open loop configuration beginning outside the chamber, passing directly through the target mount, and finally exiting the chamber with the assistance of a small vacuum pump. Heating was

performed using two 120V cartridge heaters, each 3 mm in diameter and approximately 3 cm long, inserted into the aluminium body of the target holder on opposites sides of the target. Voltage to the heaters was regulated by a PID controller and a thermocouple attached directly to the aluminium housing. This thermocouple was previously calibrated against the temperature at the centre of the foil, and thus additionally provided measure of the sample temperature just before the shot.

The resulting velocimetry data for aluminium and iron shock compressed at strain rates around 10^6-10^7 s^{-1} are shown in Fig. 1. It can be seen that for FCC Al the amplitude of the elastic precursor wave increases with temperature, whereas for BCC Fe it remains largely the same.

3. Multiscale dislocation dynamics plasticity

MDDP (Zbib and Diaz de la Rubia, 2002; Zbib et al., 2003) is a multiscale elasto-viscoplastic simulation model in which three dimensional discrete dislocation dynamics (DDD) is coupled with continuum finite element analysis (FEA). Isotropic elastic DDD computations are used to determine the plasticity of single crystals by explicit three-dimensional evaluations of dislocations motion and interaction among themselves and among other defects.

The dislocations are discretised into linear segments of mixed character, and their dynamics are governed by a mobility law describing the relationship between the segment's speed and the applied loads. In the following, the mobility of dislocations is described as (Gillis et al., 1969; Gurrutxaga-Lerma, 2016)

$$f_{PK} = \frac{d(T)}{1-\frac{v^2}{c_t^2}}v \tag{1}$$

where f_{PK} is the Peach-Koehler force applied over the dislocation segment, v the glide speed, and d the drag coefficient; c_t is the material's transverse speed of sound. The sigmoidal character of eqn. (1) with respect to v helps capturing the saturation of the dislocation's speed with increasing Peach-Koehler force as the glide speed approaches c_t.

The system is discretised into linear dislocation segments bounded by two nodes. The mobility law is applied over each segment, and the positions of the extreme nodes updated following a Galerkin formulation detailed in (Zbib and Diaz de la Rubia, 2002; Groh et al., 2009). This formulation requires resolving the value of the Peach-Koehler force over each node for each dislocation segment, which for each segment s is computed in a way analogous to the one proposed by Van der Giessen and Needleman (Van der Giessen and Needleman, 1995) for their planar model of discrete dislocation plasticity (DDP):

$$\underline{f}^s_{PK} = \left[\left(\sum_{m=1,m\neq s}^{N}\tilde{\sigma}_{ij}\right)+\widehat{\sigma}_{ij}\right]\underline{B}^s\times\xi^s \tag{2}$$

where $\tilde{\sigma}_{ij}$ is the stress field due to every other dislocation segment, $\widehat{\sigma}_{ij}$ the stress field due to the boundary conditions, $\underline{B}$ is the segment's Burgers vector, and ξ_s its orientation. The way in which MDDP computes the stress fields of the dislocations, and therefore $\tilde{\sigma}_{ij}$ is discussed in detail in (Zbib and Diaz de la Rubia, 2002). Here it suffices to say that unlike in D3P (see section 5), the fields of the dislocations solved in MDDP will be linear elastic and *quasistatic*, i.e., independent of time.

The external stress field $\widehat{\sigma}_{ij}$ is computed employing the finite element method, which is coupled to the dislocation problem using linear superposition (cfr. (Van der Giessen and Needleman, 1995; Zbib and Diaz de la Rubia, 2002; Shehadeh et al., 2005; Shehadeh, 2012)). As a result, each time step MDDP will resolve the mobility law of each dislocation segment, and advance its position accordingly, leading to the evolution of the dislocation microstructure in response to external loading. For each time step, the velocities of the dislocation segments are used to obtain the plastic strain rate $\dot{\varepsilon}^p$ and the plastic spin W^p, which are computed as the aggregate over each dislocation:

$$\dot{\varepsilon}^p = \sum_{i=1}^{N}\frac{l_i v_i}{2V}(n_i\otimes B_i + B_i\otimes n_i) \tag{3}$$

$$W^p = \sum_{i=1}^{N}\frac{l_i v_i}{2V}(n_i\otimes B_i - B_i\otimes n_i) \tag{4}$$

where v_i is the glide velocity of each segment, N is the total number of dislocation segments, n_i is the normal vector of each dislocation segment, B_i is the Burger's vector of each segment, l_i is the length of the segment, and V is the volume.

3.1. Temperature effects on dislocation mobility

Here, temperature effects are captured via the drag coefficient, $d(T)$, and via the changes in c_t with increasing temperature. The latter are summarised in Table 1 alongside the values of the elastic constants that are employed in the simulations. The former are extracted from experimental data and molecular dynamics simulations.

Table 1
Elastic properties of FCC aluminium and BCC iron at different temperatures. Data extracted from (Ho and Ruoff, 1969; Levy et al., 2000; Dever, 1972). The Burgers vector magnitude is kept constant with temperature, and is $\mathbf{B}_{Al} = \mathbf{2.85}$Å for Al and $\mathbf{B}_{Fe} = \mathbf{2.48}$Å.

Temperature	125K	293K	455K	605K	795K
FCC Al					
ρ (kg/m^3)	2713.15	2705.14	2683.82	2642.16	2607.76
E (GPa)	71.72	64.03	56.62	49.75	42.7
μ (GPa)	27.02	23.68	20.58	17.84	15.18
c_t (m/s)	3155.86	2962.2	2769.05	2593.3	2412.87
c_l (m/s)	6406.86	6288.81	6174.97	6069.57	5961.35
BCC Fe					
ρ (kg/m^3)	7975	7864	7729	7604	7500
E (GPa)	226.5	215.44	201.1	184.5	159.1
μ (GPa)	85.1	80.4	74.4	68	60
c_t (m/s)	3267.6	3197.22	3103.96	2986.74	2782.17
c_l (m/s)	6486.96	6493.59	6461.41	6385.9	6124.7

Based on conventional understanding of the effect of temperature in the phonon scattering and phonon wind effects that drive the drag coefficient (Nabarro, 1967), $d(T)$ is made to be directly proportional to temperature for both FCC Al and BCC Fe. For a specific temperature T, the drag coefficient $d(T)$ is

$$d(T) = \frac{d(T_R)}{T_R} \cdot T \tag{5}$$

where T_R is the reference temperature (hereafter, $T_R = 293$ K), $d(T_R) = 2 \cdot 10^{-5}$ Pa$\cdot$ s for FCC Al (Olmsted et al., 2005; Cho et al., 2016), and $d(293K) = 9.4 \cdot 10^{-5}$ Pa$\cdot$ s for BCC Fe (Urabe and Weertman, 1975). This applies well for the mobilities of FCC aluminium in the range of 216 – 540 K (Olmsted et al., 2005); the cases of higher and lower temperature and that of BCC Fe are extrapolated.

Moreover, it is well established that while the mobility dislocations in FCC metals is independent of the dislocation character, the mobility of edge and screw characters in BCC metals is different (Cai and Bulatov, 2004). Since the energy involved in creating a new edge segment is about 2 times as large as it is to create a screw segment (Clouet, 2009; Hull and Bacon, 2011), edge and mixed dislocation speeds can be one or even two orders of magnitude higher than the screw ones (Lawley and Gaigher, 1964; Imura et al., 1985). This effect is supported by many experimental observations which show that in BCC metals, such as Mo, the mobility of screw dislocations is 40 times less than the mobility of non-screw segments (Lawley and Gaigher, 1964); in the case of Fe, the difference in mobilities is estimated at about 80–100 (Domain and Monnet, 2005; Monnet and Terentyev, 2009; Queyreau et al., 2011). Thus, in order to model the constrained motion of screw components in BCC Fe, the MDDP model is modified to account for the difference in the drag coefficient of screw dislocations, which in the following shall be

$$d_{\text{screw}} = 100 \cdot d_{\text{edge}} \tag{6}$$

3.2. Incorporation of temperature and orientation dependent frictional stress for BCC iron

The Peierls stress of pure screw dislocations in BCC metals is very large when compared to the values exhibited by pure edge and mixed dislocations (Wang and Beyerlein, 2011; Salehinia and Bahr, 2014). For example, in Mo and Ta, the Peierls stress may exceed 1000 MPa (Li et al., 2004). This large value of lattice friction is an indication of the high energy barrier for the movement of screw dislocations which is associated with the compactness and polarisation of the screw dislocation core. The effect of the dislocation core is also reflected on the predominance of thermally and stress activated kink mechanisms, and the observation of long extended screw dislocations (cf. (Hornbogen, 1962)).

Here, MDDP has been extended to incorporate the anisotropy and temperature effect on the frictional stress in BCC metals. First, it is assumed that the lattice frictional force of the screw segments is 10 and 4 times larger than those of pure edge and mixed dislocations respectively (Wang and Beyerlein, 2011). Moreover, lattice friction is strongly temperature dependent, which is justified by high temperature sensitivity of yielding in BCC metal. Therefore, the following lattice friction model is incorporated into the MDDP framework

$$F_P(T) = F_P^{\text{edge}}(T_R) \frac{T_R}{T} Y_{\text{amp}}, \tag{7}$$

where T_R is room temperature, T the material's current temperature, $F_P^{\text{edge}}(T_R)$ is the lattice friction of a pure edge segment at room temperature. Y_{amp} is an amplification factor to account for the higher frictional stress in non-edge segments observed in BCC metals, with values of 1, 4, and 10 for pure edge, mixed, and pure screw segments respectively (Wang and Beyerlein, 2011;

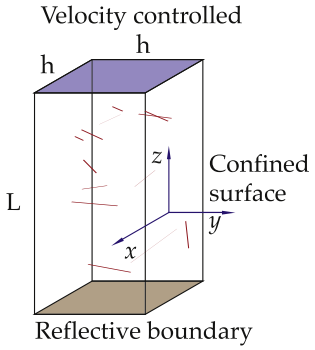

Fig. 2. MDDP simulation set up. The red segments represent the starting Frank-Read source density. (For interpretation of the references to colour in this figure legend, the reader is referred to the web version of this article.)

Itakura et al., 2012; Kubin, 2013; Monnet and Terentyev, 2009). For dislocations in FCC, it is assumed that Y_{amp} is unity regardless of the dislocation character.

The motion of dislocations is activated once the resolved shear stress over a specific dislocation segment overcomes the value of F_P. In the current simulations of BCC Fe, $F_P^{\text{screw}} = 600$ MPa at room temperature, which declines to around 220 MPa at 800K (q.v. (Gilbert et al., 2013)).

3.3. MDDP simulation set up

The MDDP simulations reported here are designed to mimic the shock compression experiments described in section 2 for FCC Al and BCC Fe shocked with a strain rate of $\approx 10^7$ s^{-1}. As can be seen in Fig. 2, the simulation domain consists of a column of length L with square cross section $h \times h$ oriented in the [001]. The dimensions of the domain are 0.5μm × 0.5μm × 24μm for Al, and 0.5μm × 0.5μm × 12μm for Fe. The shockwave is generated by applying a displacement-controlled boundary condition on the upper surface. The four sides are confined (Khan et al., 2004)[1] to achieve the uniaxial strain condition involved in planar waves, and the lower surface is a reflective boundary (i.e., rigid). The loading was such that a ramp wave of a particle velocity U_p is produced over a finite rise t_{rise} chosen based on the experimentally measured values of ≈1 ns.

Frank Read (FR) sources are randomly placed on the slip planes to act as a dislocation generation mechanism. The dislocation source length ranges between 0.25μm to 0.5μm, resulting in an initial dislocation density is in the order of 10^{12} m^{-1}. This initial value of the dislocation density is chosen to mimic the response of annealed crystals. It is worth noting that in the MDDP simulations the homogeneous nucleation mechanism is not considered; as will be argued in section 5, the magnitude of the shock load in the current work is insufficient for the plastic response to be dominated by homogeneous nucleation (cf. (Shehadeh et al., 2006; Gurrutxaga-Lerma et al., 2015b; Kattoura and Shehadeh, 2014; Shehadeh and Zbib, 2016)). All relevant material properties used in this work are summarised in Table 1.

4. MDDP simulations: results and discussion

4.1. Dynamic yielding in FCC Al at different temperatures

As the shock wave advances in Al, it interacts with the existing dislocation sources leading to their activation once the resolved shear stress exceeds the critical value to overcome the lattice fiction and the self-stress of the activated sources. As a result, loops and segments are emitted from the FR sources and accelerated to a velocity approaching the shear wave velocity almost instantaneously (Fig. 3a). Due to the isotropy in the Peierls barrier exhibited by Al, FR source activation takes places uniformly, where all parts of the source begin to bow out at the same time irrespective of their character. As the wave propagates, more sources are activated while the already activated ones continue to emit more dislocations (Fig. 3b). This process continues leading to a large increase in the dislocation density at a very high rate (Fig. 3b), thereby relaxing the shock front.

Fig. 4 depicts the longitudinal wave history computed at a deformation temperature of 293K in Al subjected to a shock wave launched with strain rate 10^7 s^{-1}. The wave history is plotted at a horizontal section taken after the wave has travelled a distance of 3μm (1/4 of the height). It is apparent that the wave profile consists of a wave front of a 1.5ns duration followed a plateau at the peak stress. By inspecting the wave front characteristics, one can see that in the first 0.7 ns, the section was still under ambient pressure condition. The stress then starts to build up in a purely elastic manner until it reaches a critical value

[1] The sides are allowed to move in the wave propagation direction, but not in the lateral (x and y) directions. This is to ensure a uniaxial loading (compression) condition.

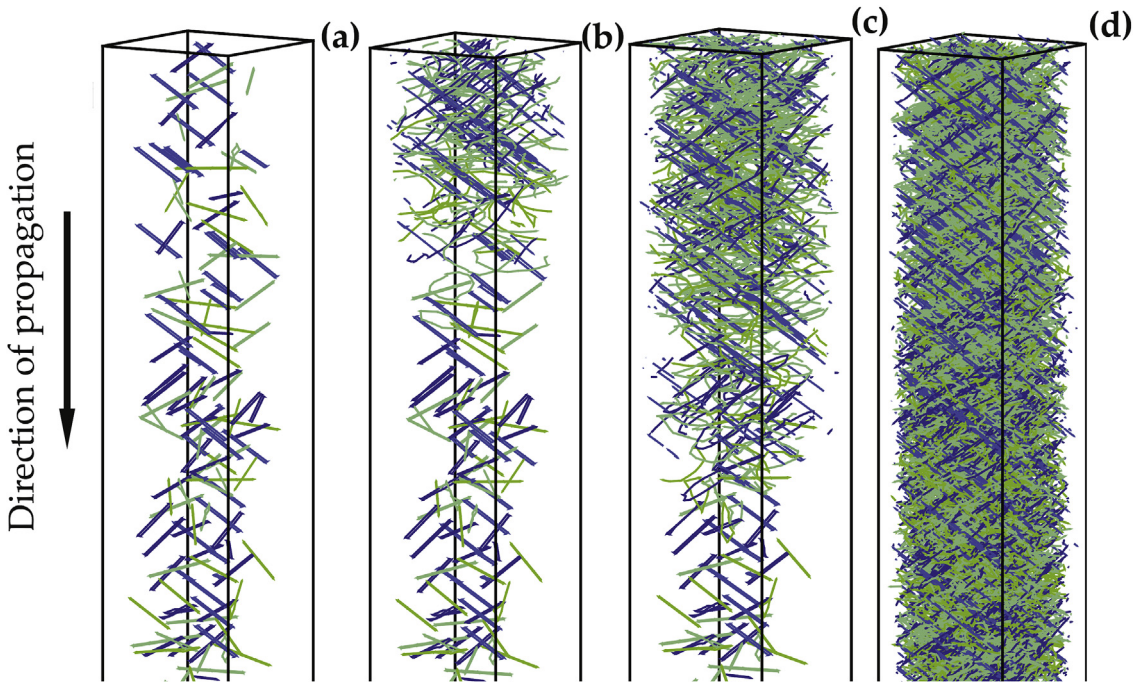

Fig. 3. Snapshots of the dislocation microstructure evolution during wave propagation. Each colour is for dislocations on a specific slip plane (a) Initial dislocation structure. (b) Shock wave is launched on the top surface with a ramp front that begins to activate the dislocation sources; (c) the wave travels in the crystal leading to activation of more source while the previously activated ones continue to emit more dislocation loops. (d) By the time the wave reaches the bottom surface, the number of emitted dislocations becomes so large that it fills the entire volume leading to huge increase in the dislocation density. (For interpretation of the references to colour in this figure legend, the reader is referred to the web version of this article.)

where a change in the slope defining the dynamic yield point is formed on the elastic front. This yielding behaviour is a manifestation of plastic relaxation that takes place due to shock-dislocation interaction. The stress continues to increase to the peak value of 10 GPa which is attained after 1.5 ns (rise time).

In order to assess the dynamic yield characteristics, we have computed the stress histories at three different locations, that is; after the wave has travelled distances of $0.25L$, $0.5L$ and $0.75L$, where L is the height of the column. As shown in Fig. 5a, by inspecting the ramp front at these locations, we observe the attenuation of the yielding point, which is attributed to the continuous stress relaxation resulting from dislocation activities as the shock wave travels through the sample volume.

The effect of deformation temperature on yielding in FCC Al is also investigated. Two additional MDDP simulations have been carried out at 605K and 795K to compare with the results obtained at 293K. As can be seen in Fig. 5b, the stress histories computed at 0.75L show two distinct features of the temperature effect on the dynamic response: (1) the time of wave arrival increases with temperature due to the decrease in the shock wave velocity; and (2) the magnitude of the dynamic yield point increases with temperature.

Fig. 6a shows the variation in the dynamic yield stress against the distance travelled by the shock wave for all simulated temperatures. The data can be approximated by a power function $s = ax^{-b}$, with a and b being 0.68 and 0.18 at 300K, 0.64 and 0.183 at 605K and 0.68 and 0.15 at 795K. The elastic precursor decay rate is associated with the parameter b, which slightly decreases with temperature. This behaviour is qualitatively similar to the experimental data presented in section 2; however, the simulation data shown in Fig. 6a is two to three times smaller than the experimental values. This is due to the fact that the experimental data are obtained after a much larger propagation distance, for shock waves which have accordingly experienced a greater degree of stress relaxation.

The temperature hardening of the dynamic yield point shown in Fig. 6b, although unusual (Hunter and Preston, 2015; Garcia-Gonzalez et al., 2017; Lim et al., 2015), is entirely consistent with dislocation theory. Although at low strain rates yielding is associated with the thermal activation of the motion of dislocations (Hirth and Lothe, 1982), at the higher strain rates such as those probed here, plastic slip is expected to be dominated by viscous drag, which is well-known to increase linearly with temperature; this is confirmed by the MDDP simulation results shown in Fig. 6b, and the experimental data gathered in (Kanel et al., 2003; Zaretsky and Kanel, 2012) and in section 2, all of which show a linear increase of the shear stress increases with temperature.

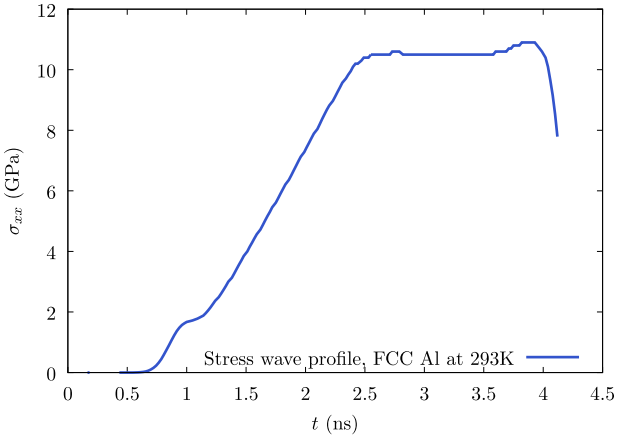

Fig. 4. Stress history in a section taken at the upper part of the MDDP sample, for a travelled distance of about 3μm.

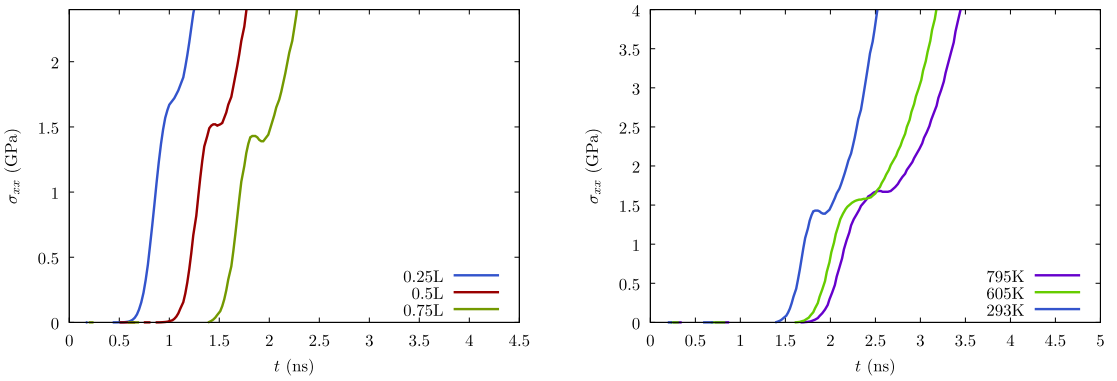

(a) Stress history in different sections of the FCC Al sample shocked at 293K.

(b) Stress wave profiles at $0.75L$ at 293K, 605K and 795K.

Fig. 5. Stress history taken at different sections of the FCC Al MDDP system.

4.2. *Dynamic yielding in BCC Fe at different temperatures*

The effect of temperature on the dynamic yielding in BCC iron is also investigated using the MDDP framework. The simulation setup is identical to that of Al, but with double the height along the direction of propagation of the shock wave (see Fig. 2). As discussed in section 4.2, lattice friction in BCC metals is assumed to be both dislocation character and temperature dependent.[2]

Fig. 7 shows snapshots of the dislocation evolution in iron subjected to room temperature deformation at a rate of 10^7 s^{-1}. In contrast to what occurs in FCC Al, dislocation activation in Fe commences by the emission of pure edge segments that sweep through the crystal, leaving behind trails of extended screw segments, which can be clearly seen in Fig. 7 and, on a closer look, in Fig. 8. These extended screw lines stay sessile until the resolved shear stress becomes high enough to move them. The formation of these extended lines is attributed predominantly to the large Peierls barrier of screw dislocations in BCC Fe. As the stress builds up on the wavefront, the critical value to overcome the lattice friction of the screw segments is reached, enabling their movement and thus additional stress relaxation. By closely examining the activated dislocations, one

[2] Although the ratio of lattice frictions between screw and non screw segments (Y_{amp}. in eqn. (7)) employed here was 10 and 4 for pure edge and mixed segments respectively, other combinations such as 100 and 40 were tried, and the change in results seems to be insignificant. However, the lack of a significant lattice friction for screw components resulted in a qualitative behaviour very similar to that of FCC Al, which suggests that lattice friction hindering the motion of screw dislocations plays a fundamental role in the behaviour described in the following.

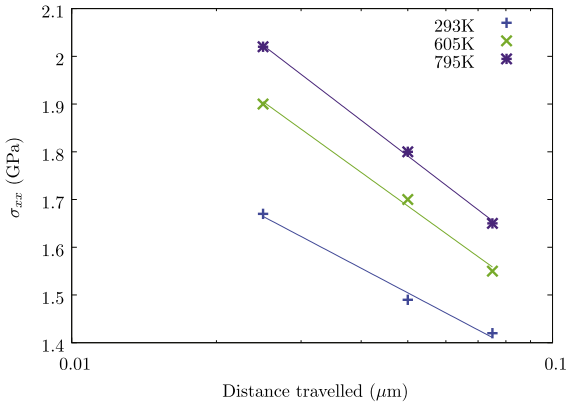

(a) Magnitude of the precursor peak (the dynamic yield point) at different sections, for FCC Al.

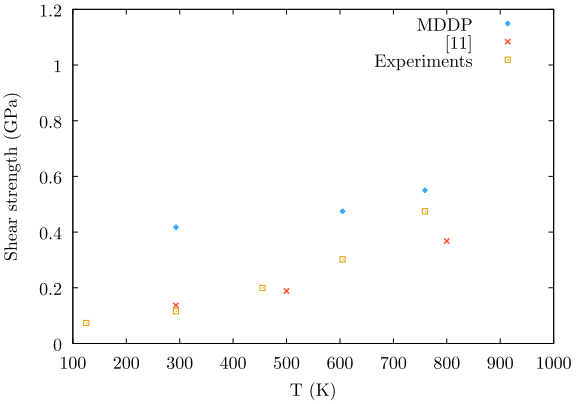

(b) Shear strength for FCC Al: experiment vs simulations.

Fig. 6. Effect of temperature in the attenuation of the dynamic yield point.

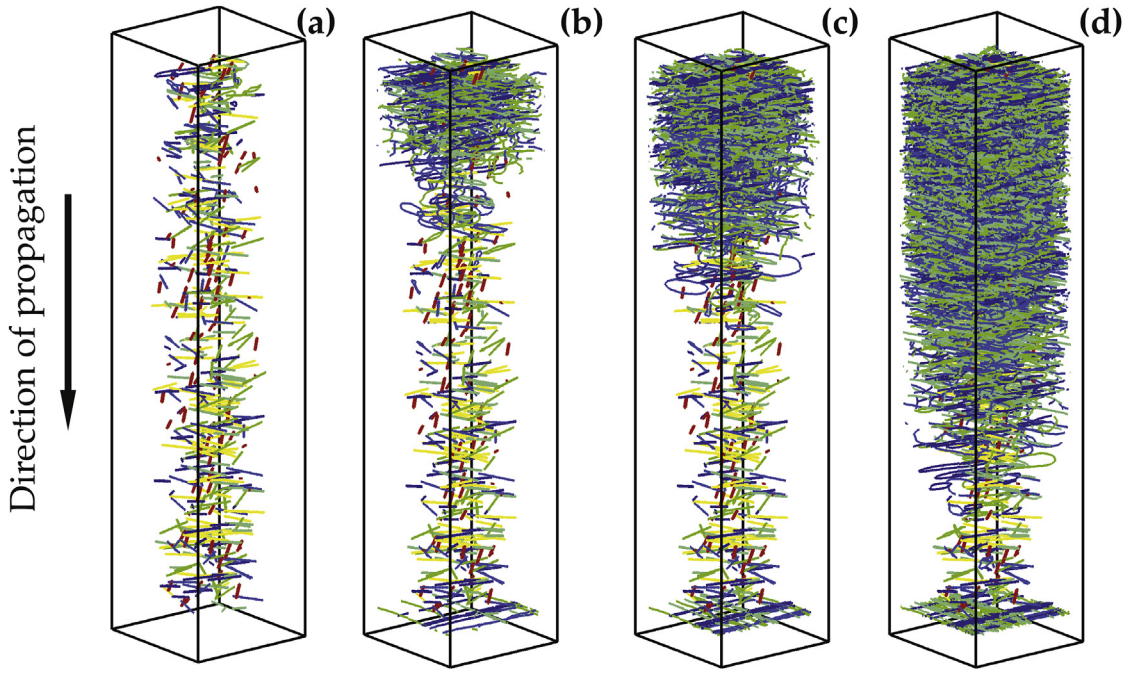

Fig. 7. Snapshots of the dislocation microstructure evolution during wave propagation in Fe. Each colour corresponds to dislocations on a specific slip plane: (a) Initial dislocation structure; (b) Shock wave is launched on the top surface with a ramp front that begins to activate the dislocation sources, some FR sources are not activated (red colour) as they reside on slip planes of zero Schmid factor; (c) the wave travels in the crystal leading to activation of more source while the previously activated ones continue to emit more dislocation loops; (d) by the time the wave reaches the bottom surface, the number of emitted dislocations becomes large, leading to huge increase in the dislocation density. (For interpretation of the references to colour in this figure legend, the reader is referred to the web version of this article.)

can see that the movement of these screw segments is dominated by kink or double kink mechanism as illustrated in Fig. 8. Such dislocation microstructure has been previously observed in BCC Fe subjected to shock loading (Hornbogen, 1962).

The longitudinal stress histories during the wave passage in Fe are depicted in Fig. 9a. Similar to FCC Al, the elastic precursor peaks at the dynamic yield point, which is continuously attenuated during wave propagation. Fig. 9b compares MDDP computed values of the dynamic yield point after the wave has travelled 15μm at different temperatures with reported

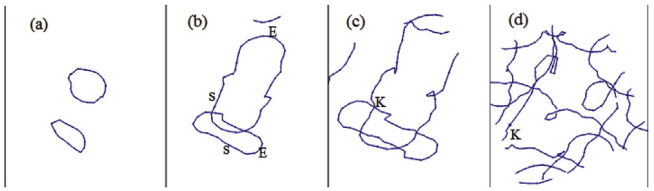

Fig. 8. Closer look at the dislocation evolution during the initial steps of loading. Here we show (a) two Frank-Read sources placed on one of the (101) planes; (b) Source activation with the edge segments (E) move at high speed leaving behind sessile extended screw segments (S), (c and d) The resolved shear stress becomes high enough to allow the motion of the screw segments via kink formation (K).

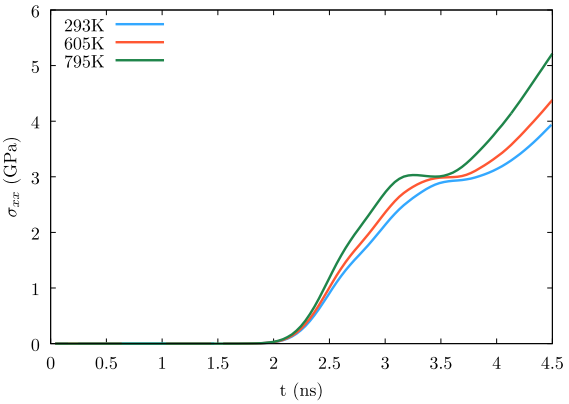

(a) Dynamic yield point of BCC Fe for different temperatures after the wave has propagated 10μm.

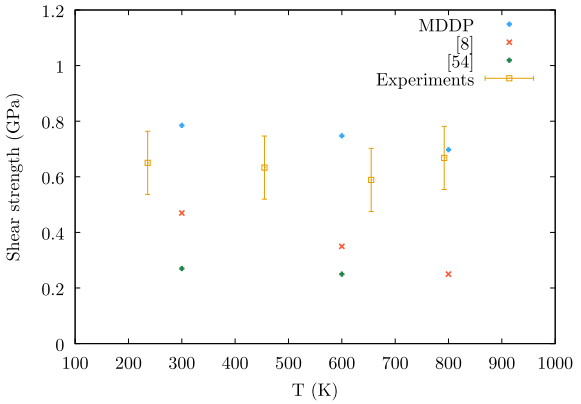

(b) Simulated vs experimentally measured shear strength of BCC Fe at different temperatures.

Fig. 9. Effect of temperature in the attenuation of the dynamic yield point of BCC Fe. The trends are similar in all cases, and the differences in magnitude can be accounted for by differences in the location within the sample the shear strength was measured (i.e., different experimental sample thicknesses).

experimental data. In contrast with the response of Al, the dynamic yield point of Fe remains largely insensitive to increases in temperature (even showing a slight decrease), suggesting that the dislocation drag hardening expected with increasing temperature is somewhat counterbalanced by the drop in the Peierls barrier and enhanced dislocation density. This trend is consistent with the experimental findings reported in section 2, and with previous work on BCC Fe subjected to similar loading ranges, where either temperature insensitive yielding (Rohde, 1969) or even a slight decline in plastic yielding (Zaretsky, 2009) was reported. The larger magnitude of the yield point found in MDDP (and in different experiments) can be attributed primarily to the difference in the distance travelled by the shock front before measurement, so the further away from the impact surface the measurement is performed, the lower the yield point's magnitude ought to be.

5. A D3P analysis of shock loaded iron and aluminium at different temperatures

The MDDP model presented in section 4 highlights the importance dislocation mobility has in the plastic relaxation process of both Al and Fe. For Al, the enhanced mobility of edge dislocations relative to screw dislocations appears crucial in producing the required degree of plastic relaxation at the front. Increasing the temperature hinders the motion of the edge components and, crucially, that of screw components even more; ultimately, this results in the increase in the dynamic yield point of Al. For Fe, the drag coefficients are larger, and the motion of screw components is severely limited by much larger Peierls barriers; increasing the temperature does not result in an appreciable change of the yield point because the mobility of dislocations is already compromised to begin with.

Thus, the MDDP analysis relates enhanced or hindered dislocation mobilities with increased or decreased yield points. However, dislocation mobility on its own does not cause plastic yielding; rather, plastic yielding at the front is caused by the applied load and the elastodynamic fields of dislocations, which negatively interfere with the front, thereby attenuating it. In that sense, while MDDP is very useful in explaining the mesoscopic aspects of the shock-induced plasticity, it cannot provide a

detailed analysis of shock front relaxation, because it is a quasi-static method where the fields of dislocations (and therefore their interactions with one another and with the medium) are insensitive to the dislocation's speed.

The aim of this article is to offer an interpretation of the process leading to the attenuation of the dynamic yield point at different temperatures in both Al and Fe, by focusing on what happens at the onset of plastic flow in the shock front. In order to do that, *Dynamic Discrete Dislocation Plasticity* (D3P), a fully time-dependent, elastodynamic planar model of discrete dislocation dynamics, will be employed. By using D3P, the effect of dislocation speed in the fields of the dislocations is naturally captured, which will lead to a mechanistic interpretation of the effect of temperature in the dynamic yield point.

5.1. D3P vs MDDP

The D3P model presented here is based on the work of Gurrutxaga-Lerma et al. (2013; 2014; 2015b). The model arises as the elastodynamic extension to *Discrete Dislocation Plasticity* (DDP) (Van der Giessen and Needleman, 1995). As in DDP, D3P concerns only to plane strain situations, and therefore only deals with individual edge dislocations, which are treated as infinite and straight. The use of a planar method to analyse the relaxation of the shock front is in this case doubly justified. On the one hand, the expected applied loading in the experiments reported in section 2 is, to a good approximation, plane strain; on the other hand, the MDDP simulations have highlighted the dominant role that edge components have in the relaxation of the shock front, whereby screw dislocations appear mostly as debris behind the front; this is corroborated by prior experiments (Hornbogen, 1962; Meyers et al., 2009).

Aside from the planarity, the main difference between D3P and MDDP is that D3P deals with individual edge dislocations in a planar *elastodynamic* continuum, whilst in MDDP the continuum is *elastostatic*. This means that unlike MDDP, D3P fully incorporates inertial effects into both the motion and the interactions of the dislocations: interactions of dislocations with one another and with the medium will be based on a retardation principle, and depend on the time it takes for elastic perturbation waves to travel from the core of a dislocation to other defects or the boundaries of the domain. As a result, it provides a much more fine grained account of the way dislocations behave in the shock front. Thus, although as a planar method D3P cannot perform detailed analyses of forest hardening, cross-slip or other phenomena where mixed or screw dislocation lines play a crucial role (all of which are modelled in MDDP), it recovers causality and provides a much greater deal of accuracy in instances such as the study of the shock front, where those phenomena have little effect. Further details on the way the D3P model works can be found in (Gurrutxaga-Lerma et al., 2013, 2014).

Here, the D3P model will therefore be employed to study the way in which the dislocations mediate to relax the shock front at different temperatures.

5.2. D3P model set up

The modelling system is shown in Fig. 10. Its dimensions must be wide enough to accommodate a shock front of 10^7 s^{-1}. This manifests in the experimental test samples the D3P model will be compared with, the width of which was 125 μm. A simulation of such width in D3P would be computationally intractable, so here the size of the D3P system is reduced to a 25 μm wide and 0.5 μm tall sample, which will accommodate the propagating front over approximately 4ns. Upon arrival at the rear surface, the simulation is terminated, so this surface is simulated as a reflective boundary. In the D3P simulations, the shock wave is launched by suddenly applying a a distributed load of 5.5 GPa over the impact surface (see Fig. 10). The strain rate is controlled numerically. As it propagates through the sample, dislocation activity will be triggered, and plasticity will ensue. Due to the aspect ratio of the experimental sample (see section 2), rarefaction waves coming from the free surfaces (excluding the rear surface, where measurements are made) are unlikely, so the D3P system will exclude those surface effects by imposing periodic boundary conditions on the top and bottom surfaces (see Fig. 10); the resulting shock wave will accordingly resemble a planar front.

In D3P dislocations are treated as point-like particles that move in preferential directions: the slip planes. For plane strain, the crystallography of the material is reflected with slip planes at $\pm 54.7^\circ$ and 0° for FCC Al, and $\pm 35.3^\circ$, 90° for BCC Fe (Rice, 1987); the angles are measured with respect to the direction of propagation of the shock wave, which in this case therefore advances in the [101] direction (cf. (Hirth and Lothe, 1982; Franciosi et al., 2015)). Since the loading is strongly uniaxial, both

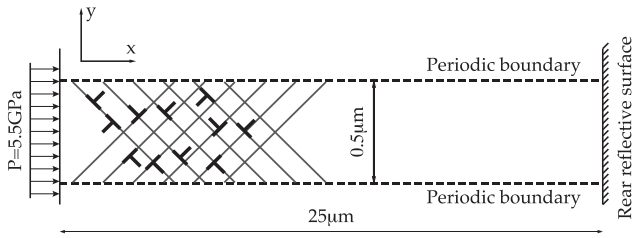

Fig. 10. Schematic of the D3P system's geometry, where x is the direction of propagation of the shock wave.

the 0° and 90° slip planes are unlikely to be activated by anything other than other dislocations, because the applied resolved shear stress is zero.

As in MDDP, D3P relies on the principle of linear superposition to resolve interactions between dislocations and between dislocations and the boundaries (cf. (Van der Giessen and Needleman, 1995)). As shown in Fig. 11, the domain is decomposed into an infinite plane, $\tilde{\Omega}$, and a boundary value problem $\widehat{\Omega}$. The analytic expressions for the elastodynamic fields of an injected, non-uniformly moving dislocation (found in (Markenscoff and Clifton, 1981; Gurrutxaga-Lerma et al., 2013)) are employed to compute interactions between dislocations on the $\tilde{\Omega}$ domain, whilst the boundary value problem in $\widehat{\Omega}$ is solved numerically, employing an explicit finite element solver. In both cases the field equation is the fully time-dependant Navier-Lamé equation (vid. (Achenbach, 1973)): this enables the propagation of a shock wave in $\widehat{\Omega}$, and the elastodynamic interactions between dislocations in $\tilde{\Omega}$. Closure is offered via the tractions and displacements, that are computed on the boundary of $\tilde{\Omega}$ and applied with reversed sign in $\widehat{\Omega}$. Dislocation interactions are resolved naturally via the Peach-Koehler force, which is computed as in section 4, but applied to straight edge dislocations in the plane (vid. (Van der Giessen and Needleman, 1995)):

$$f^s_{PK} = n^s_k \left(\sum_{j \neq s} \tilde{\sigma}^j_{kl} + \widehat{\sigma}_{kl} \right) B^s_l \tag{8}$$

where for dislocation s f^s_{PK} is the glissile component of the Peach-Koehler force, n^s_k is the normal to the slip plane, B^s_l the Burgers vector; $\tilde{\sigma}^j_{kl}$ is the elastodynamic stress field of dislocation j, and $\widehat{\sigma}_{kl}$ the elastodynamic stress field correction due to the boundary conditions in the $\widehat{\Omega}$ field.

Results will be analysed as detailed in (Gurrutxaga-Lerma et al., 2015b), by averaging the σ_{xx} stress component over sections perpendicular to the direction of propagation of the front. The elastic precursor peak is identified when the activity of the fields of dislocations becomes significant for the first time.

5.3. Temperature and the mobility of dislocations

As in MDDP, the mobility of dislocations is described with eqn. (1) (vid. (Gurrutxaga-Lerma, 2016)):

$$f^s_{PK} = \frac{d(T)}{1 - \frac{v_s^2}{c_t^2}} v_s \tag{9}$$

where f^s_{PK} is the glissile component of the Peach-Koehler force, in the planar case given by $f^s_{PK} = B \cdot \tau$ (with τ is the applied resolved shear stress, B the Burgers vector) (Hirth and Lothe, 1982), v_s the glide speed of the s-th dislocation, and $d(T)$ the drag coefficient. Here, temperature effects are captured via the drag coefficient which will be described as was done in section 4 for MDDP in eqn. (5):

$$d(T) = \frac{d(T_R)}{T_R} \cdot T \tag{10}$$

The same values of $d(293K) = 2 \cdot 10^{-5}$ Pa· s and $9.4 \cdot 10^{-5}$ Pa· s for Al and Fe respectively will be used, as in section 4 (see (Olmsted et al., 2005; Queyreau et al., 2011; Yanilkin et al., 2014)).

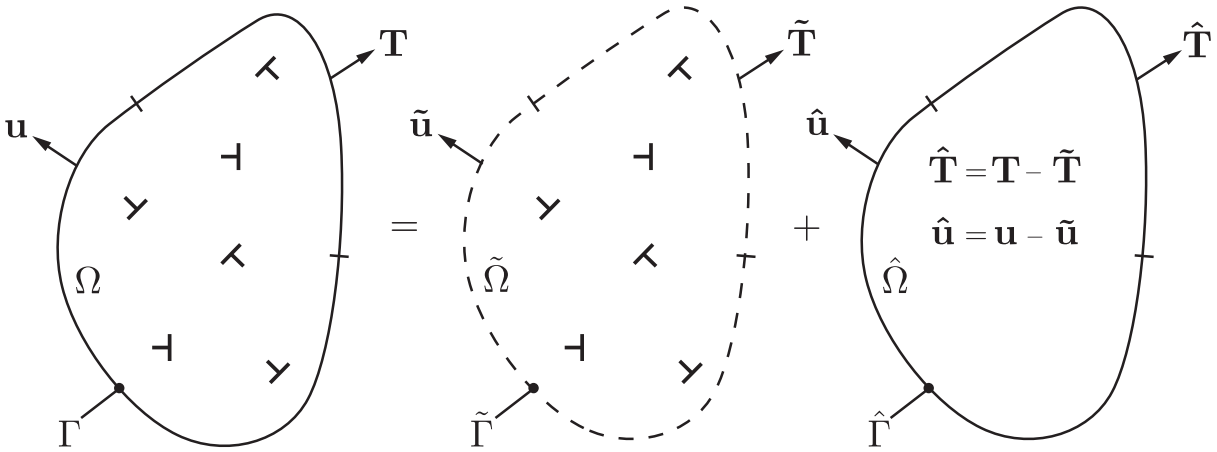

Fig. 11. The boundary value problem, using a linear superposition scheme. After (Gurrutxaga-Lerma et al., 2013).

As discussed in section 4, the mobility law is affected by temperature both via variations in the drag coefficient and the transverse speed of sound c_t: the limiting speed of dislocations (the transverse speed of sound) decreases with temperature (see Table 1). The result of increasing the temperature is lower glide speeds for equal applied stress levels. The resulting dislocation mobilities are shown in Fig. 12. The present simulations do not account for changes in the values of the elastic constants with pressure, which are deemed to be relatively small compared to the effect of temperature (Becker, 2004). Equally, local heating due to moving dislocations (see (Gurrutxaga-Lerma, 2017)) is neglected.

5.4. Temperature and source activation

Since increasing the temperature of the material results in decreasing the value of the elastic constants of the material and, at the same time, increasing the dislocation drag, this will affect the activation of dislocation sources in the material. Following (Gurrutxaga-Lerma et al., 2015b), two kinds of sources of dislocations are allowed: Frank-Read sources and homogeneous generation.

5.4.1. Homogeneous nucleation

Homogeneous generation of dislocations is implemented by following the rules described in Gurrutxaga-Lerma et al. (2015) (Gurrutxaga-Lerma et al., 2015c). Upon overcoming a threshold stress of $\tau_{\text{nuc}} = \mu/(4\pi)$, a dipole is instantaneously injected (i.e., injected during the same time step the source is activated); this threshold stress corresponds with the theoretical lattice shear strength of the material, usually assumed to be somewhere between $\mu/(4\pi)$ and $\mu/18$. It must be noted that the dislocation's core cut-off distance is chosen to be $r_c = 10$ B; the radial stress within the core matches that at the cut-off distance (Gurrutxaga-Lerma et al., 2013). This ensures that the stresses within the core always remain below the lattice shear strength; thus dislocations can only (albeit unlikely) generate other dislocations homogeneously through long-range interactions—this ensures that avalanches of homogeneously nucleated dislocations do not take place. The homogeneous injection distance (i.e., the separation between the two dislocations in the newly injected dipole) follows a rare event Poisson distribution with $\lambda = 5B$ (where λ is the expected value), which entails that some dipoles collapse back onto each other. Any point in the material subjected to these stresses is considered a possible nucleation site, albeit the nucleation sites are spaced $10B$ to prevent newly injected dipoles from overlapping. This exclusion zone only applies to lattice locations, and remains unaffected by the presence of a dislocation.

As expected (cf. (Cahn, 1957; Hirth and Lothe, 1982; Tschopp and McDowell, 2008)), increasing the temperature facilitates the homogeneous nucleation of dislocation because the shear modulus μ decreases with temperature; as can be deduced from Table 1, the threshold stress τ_{nuc} falls by about 50% within the $125 - 795$ K range for both Al and Fe. Additional effects related to the thermal activation of homogeneous nucleation at high temperatures (vid. (Hirth and Lothe, 1982)) are not considered in the current model, but will likely lead to enhanced homogeneous nucleation at higher temperatures.

5.4.2. Frank-Read sources

In planar dislocation dynamics, Frank-Read sources are the main source of initial dislocation densities, and their activity is directly linked to the onset of plastic yielding (Van der Giessen and Needleman, 1995). Since they provide an inherent threshold stress to dislocation activity, they play a mechanistic role similar to the Peierls barrier in 3D dislocation dynamics: they condition the onset of plastic flow, which in both cases is governed by a temperature dependent threshold. In fact, it is

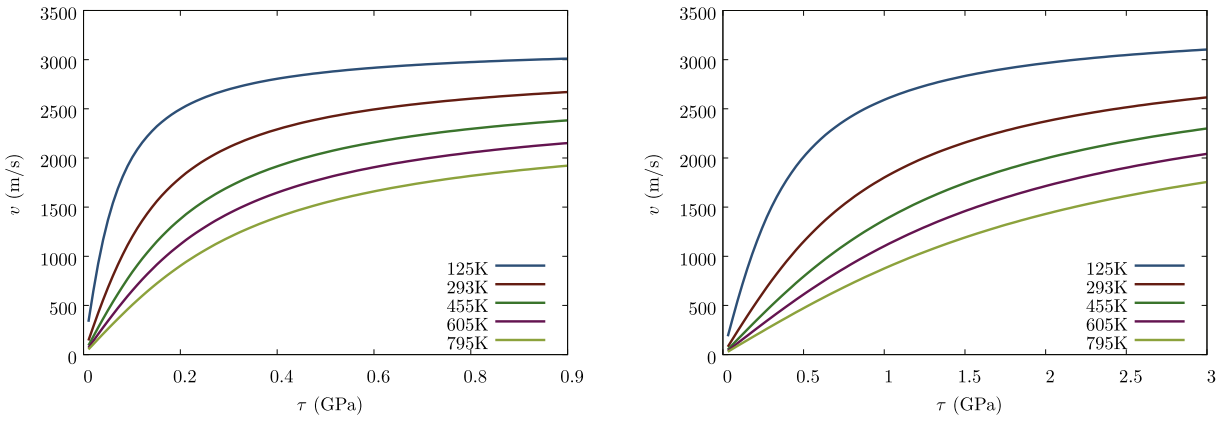

Fig. 12. Effect of increasing the temperature over the mobility of dislocations in aluminium and iron. Higher temperatures result in lower glide speeds for equal applied stresses.

well-known that both barriers are strongly correlated (Hirth and Lothe, 1982): the Peierls barrier affects 3D Frank-Read sources, and it is the latter that provides the material with its initial dislocation density. Here, Frank-Read sources are modelled as randomly distributed point sources with a density 100 sources per μm^2 (cf. (Cleveringa et al., 1999; Balint et al., 2005, 2006; Benzerga, 2009; Davoudi et al., 2014; Nicola et al., 2001, 2003)). The Frank-Read sources represent a pre-existing density of pinned dislocation segments, which enable yielding once the resolved shear stress over a source exceeds the source strength, τ_{FR}, which is the stress required for a Frank-Read source segment to reach its critical position (see (Benzerga, 2008, 2009; Shishvan and Van der Giessen, 2010; Cui et al., 2014; Gurrutxaga-Lerma et al., 2015a)). The source strength τ_{FR} is shown to be inversely proportional to the Frank-Read source segment length (Brown, 1964; Shishvan and Van der Giessen, 2010):

$$\tau_{FR} = \beta \frac{\mu B}{l_{FR}} \tag{11}$$

where l_{FR} is the segment's length, μ the shear modulus, B the magnitude of the Burgers vector and β a material-dependent parameter said to be of the form (Foreman, 1967)

$$\beta = \frac{C_1}{2\pi}\left[\ln\frac{l_{FR}}{r_0} + C_2\right] \tag{12}$$

where $C_1 = 1$, $C_2 = -3.4$ for FCC aluminium (Gurrutxaga-Lerma et al., 2015a), $C_1 = 1$, $C_2 = 0.5$ for BCC Fe, and $r_0 = 2B$ a core cut-off (Brown, 1964). Eqn. (11) states that the Frank-Read source strength is proportional to μ, so it will decay with increasing temperature, thereby making Frank-Read source activation easier at higher temperature.

The source length l_{FR} is assumed to follow a log-normal distribution (Shishvan and Van der Giessen, 2010), thereby rendering τ_{FR} normally distributed. In both the FCC Al and BCC Fe simulations considered here, the distribution of Frank-Read source lengths is chosen so that at 293K the mean strength is $\overline{\tau}_{FR} = 100$ MPa and standard deviation $\sigma_{FR} = 10$ MPa. The distribution of strengths and standard deviations at different temperatures is collected in Table 2, based on the variation of μ with temperature.

The source strength must be exceeded for a sufficiently long time called the *nucleation time*, t_{nuc}, for the source to be activated. The nucleation time of Frank-Read sources reflects the dynamics of the bowing Frank-Read source segment (Benzerga, 2008; Zhu et al., 2014; Gurrutxaga-Lerma et al., 2015a), corresponding to the time it takes for the outermost segment to reach the source's critical position (Gurrutxaga-Lerma et al., 2015a). This time is dependent on the applied load, the strain rate $\dot{\varepsilon}$ and the dislocation drag, and computed as a force balance between the Peach-Koehler force, the drag force and the line tension on the outermost segment of the Frank-Read source, the position of which is tracked via the $h(t)$ variable measuring its distance to the unbowed position, so that the nucleation time is computed as the time t when $h(t) = l_{FR}/2$, where $l_{FR}/2$ is the critical position of the loop; following (Gurrutxaga-Lerma et al., 2015a), and in agreement with the mobility law given in eqn. (1), the aforementioned force balance is expressed as

$$\underbrace{\tau(t)B}_{\text{Peach–Koehler force}} = \underbrace{\frac{d}{1-\frac{1}{c_t^2}\left(\frac{dh}{dt}\right)^2}}_{\text{Drag coefficient}} \underbrace{\frac{dh}{dt}}_{\text{Glide speed}} + \underbrace{\frac{\mu B^2}{\frac{h(t)}{2}+\frac{l_{FR}^2}{8h(t)}}}_{\text{Line tension}} \tag{13}$$

where $\tau(t)$ is the time-dependent resolved shear stress. For a constant ramping up strain rate, $\tau(t) = \mu\dot{\varepsilon}t$.

As shown by Gurrutxaga-Lerma et al. (2015a), the nucleation time expected from eqn. (13) has the proportionality

$$t_{nuc} \propto \frac{d}{\mu} \tag{14}$$

Since μ decreases and d increases with temperature, the nucleation time of Frank-Read sources is expected to increase with temperature. This is confirmed in Fig. 13, which shows the t_{nuc} resulting from the numerical solution of eqn. (13) for a loading with a constant strain rate of $\dot{\varepsilon} = 10^7\ s^{-1}$. In both the case of Al and Fe, sources of the same strength τ_{FR} show longer

Table 2
Frank-Read source strength average $\overline{\tau}_{FR}$ and standard deviation σ_{FR} for different temperatures.

Temperature	125K	293K	455K	605K	795K
FCC Al					
$\overline{\tau}_{FR}$ (MPa)	114.1	100	86.9	75.34	64.1
σ_{FR} (MPa)	11.41	10	8.69	7.53	6.41
BCC Fe					
$\overline{\tau}_{FR}$ (MPa)	105.84	100	92.54	84.57	67.62
σ_{FR} (MPa)	10.58	10	9.254	8.46	6.76

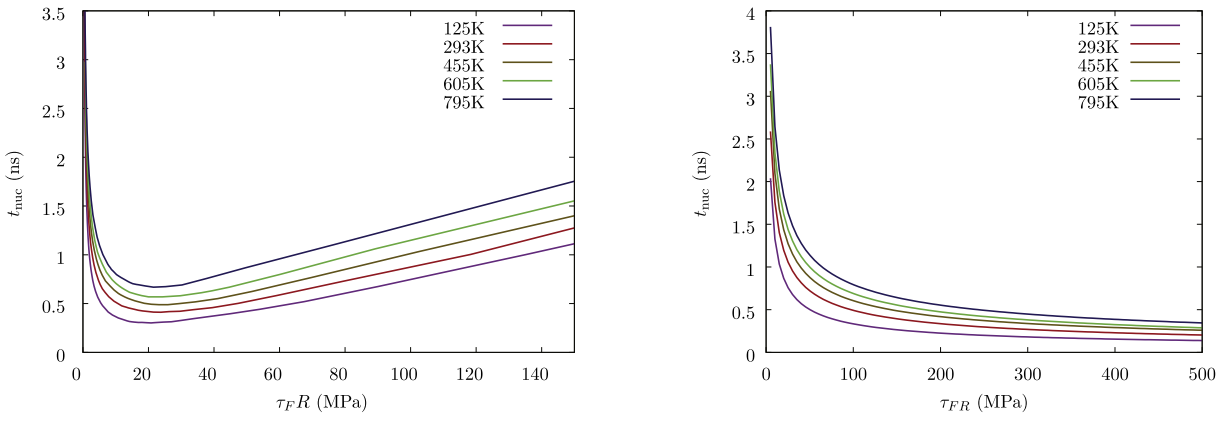

(a) Activation times for Al (b) Activation times for Fe

Fig. 13. Nucleation time of Frank-Read sources of different strength. The minima displayed in the solution is related to the nature of the loading, here assumed to be a constant strain rate 10^7 s^{-1}.

nucleation times with increasing temperature. However, excluding very low intensity sources,[3] the source activation times evolve differently with increasing τ_{FR}: for FCC Al, stronger sources always take longer time to activate; whilst for BCC Fe stronger sources invariably take shorter times to activate. As a result, increasing the temperature will not make Frank-Read sources in FCC Al activate faster; however, it will in sources in BCC Fe. Similarly, albeit in both cases increasing the temperature leads to longer activation times, in BCC Fe these longer times are relatively shorter and less sensitive to temperature.

Once the τ_{FR} has been overcome for the corresponding t_{nuc}, a dislocation dipole is injected into the system. The dislocations are injected into the system with a separation distance l_{FR} from one another chosen so as to balance their mutually attractive force with the applied resolved shear stress, τ (Gurrutxaga-Lerma et al., 2015a):

$$L_{\mathrm{FR}} = \frac{-3b^4B\mu\sqrt{\vartheta^2-a^2}+12b^2B\vartheta^2\mu\sqrt{\vartheta^2-a^2}-8a^2B\vartheta^2\mu\sqrt{\vartheta^2-b^2}-12B\vartheta^4\mu\sqrt{\vartheta^2-a^2}+8B\vartheta^4\mu\sqrt{\vartheta^2-b^2}}{-2a^2B\vartheta^2\mu\sqrt{\vartheta^2-b^2}-\pi b^2\vartheta\tau\sqrt{\vartheta^2-a^2}\sqrt{\vartheta^2-b^2}+2B\vartheta^4\mu\sqrt{\vartheta^2-b^2}} \tag{15}$$

where $a = 1/c_l$ and $b = 1/c_t$ are the slownesses of sound, and $\vartheta = 1/v$ is the inverse of the dislocation's speed, which is resolved from eqn. (1) for both Al and Fe.

The model of Frank-Read sources employed here therefore renders sources that are weaker at higher temperature, but that for the same strength take longer to activate due to the increase in dislocation drag; at the same time, stronger sources are activated faster in BCC Fe at higher temperatures. As is discussed in section 5.5, in FCC Al these two opposed effects balance each other, resulting in similar levels of plastic relaxation due to Frank-Read sources; whilst in BCC Fe, the net result is that stronger sources become more easily activated, leading to a relative increase in the number of dislocations available at the shock front.

5.5. Discussion

The increase in temperature has two effects: increasing the dislocation drag and lowering the threshold stress for nucleation of dislocations. If one considers Orowan's equation (Orowan, 1940), whereby the macroscopic strain rate $\dot{\varepsilon}$ is proportional to the average glide speed of dislocation, $\bar{v}$, and the density of mobile dislocations, ρ_m, as follows

$$\dot{\varepsilon} = \rho_m \bar{v} B, \tag{16}$$

this suggests that: (1) an increase in temperature ought to lead to a relatively larger amount of dislocation generation and, consequently, a larger degree of plastic relaxation at the shock front; and (2) that plastic relaxation may be impaired by the increased dislocation drag and the consequent drop in the average speed of dislocations. Thus, one must explore both the role of dislocation generation and dislocation mobility when varying the system's temperature.

As shown in Fig. 14, the dislocation density generated at the shock front is comparable for each temperature tested in FCC Al, whilst for BCC Fe we report a relative increase in the density; albeit homogeneous nucleation was allowed in both

[3] where the nucleation time is expected to be very large simply because the bowing segment has a very long distance to travel before reaching the critical configuration.

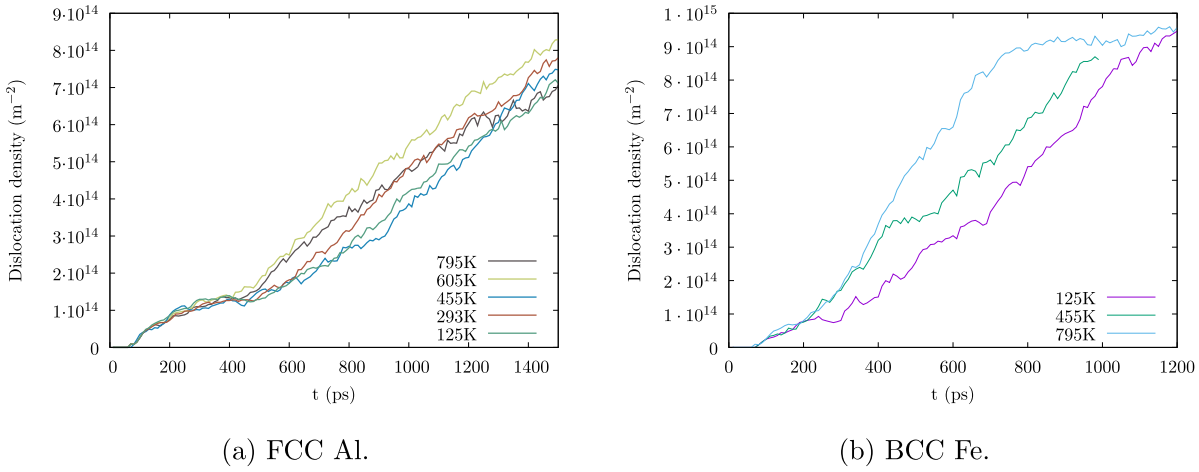

Fig. 14. Evolution of the dislocation density with temperature for the FCC Al and BCC Fe D3P samples shocked at 10^7 s^{-1}.

materials, it remains negligible in these simulations: in FCC Al, homogeneous nucleation accounts only for around $1-5\%$ of nucleation events irrespective of temperature, and seems localised at the rear end of the shock front; for BCC Fe, where homogeneous nucleation barriers are much larger, it is not observed. Frank-Read source activity is slightly different for FCC Al and BCC Fe. For FCC Al, albeit the source strength decreases with increasing temperature, the nucleation time increases due to increased drag; this entails that, as can be confirmed in Fig. 14, the net amount of dislocation generation activity over a period of time is kept within the same order of magnitude for all temperatures tested here and, therefore, that the observed differences in the amount of plastic relaxation at the front cannot be attributed to dislocation generation but, rather, to dislocation motion. For BCC Fe, the former largely applies as well. However, since the nucleation time of increasingly stronger sources decreases with source strength, the increase in temperature makes stronger sources more readily available to relax the shock front; this results in a relative increase in the dislocation density at the shock front which, as will be seen, helps in explaining the observed attenuation of the dynamic yield point.

Regarding dislocation mobility, in the D3P simulations reported here the dislocations generated at the shock front (via Frank-Read source) tend to quickly achieve glide speeds in excess of $\approx 80\%$ of the transverse speed of sound for both Al and Fe. This occurs irrespective of the temperature, because newly generated dislocations at the front are driven mainly by the unrelaxed, large magnitude shock wave. As seen in Table 1, the increase in temperatures over the 125K–795K range leads to a drop in the transverse speed of sound of about 25% for either material, which is reflected in the mobility of dislocations (Fig. 12). However, even if the dislocations keep moving at speeds in excess of 80% of the transverse speed of sound, the absolute magnitude of their speed will decrease. Thus, increasing the temperature results in increasingly lower glide speeds for the dislocations relaxing the shock front, which following the Orowan equation would entail a diminished rate of plastic relaxation per dislocation.

However, this alone does not appear to suffice to explain the observed behaviour: the shock front is not, after all, relaxed by the speed of dislocations. As was shown by Gurrutxaga-Lerma et al. (2015b), the plastic relaxation of the shock front is due to destructive interferences in the elastodynamic fields of dislocations generated at the front: the moving dislocations radiate elastodynamic waves that interfere and tend to shield the shock front. The faster that dislocations move *relative* to the transverse speed of sound, the larger the magnitude of the relaxation achieved at the front will be, and thus the larger the attenuation of the yield point will be (vid. (Gurrutxaga-Lerma et al., 2015b)). The mathematical form of the elastodynamic fields (vid. (Gurrutxaga-Lerma et al., 2013, 2014)) is such that in this regard the absolute magnitude of the dislocation's glide speed is entirely secondary to its value relative to the transverse speed of sound.

This can be observed in Fig. 15, which depicts the σ_{xx} stress component of a dislocation that, at two different temperatures (125K and 795K), was injected at $(0,0)$ and moved along a slip plane at 45° with a uniform glide speed of 90% of the speed of sound; the same instant in time ($t = 145$ ps) is represented for both temperatures. Had the dislocation been generated in a longitudinal shock front moving frontward, the main part of the σ_{xx} stress field responsible for the plastic relaxation of the shock front would be the one ahead of the dislocation core (i.e., the $x>0, y>0$ quadrant in Fig. 15). The differences in the magnitude of the speeds of sound, lower at 795K than at 125K, are responsible for the smaller size of both the transverse and longitudinal injection fronts (the two concentric circles signifying the arrival time of the longitudinal and transverse components of the stress field of the injected, uniformly moving dislocation). However, no appreciable change in the Doppler contractions and dynamic magnification of the fields are observed in Fig. 15; any change in the magnitude of the fields and, therefore, in the magnitude of the plastic relaxation, are due to the change in the magnitude of the shear modulus μ that modulates these plots.

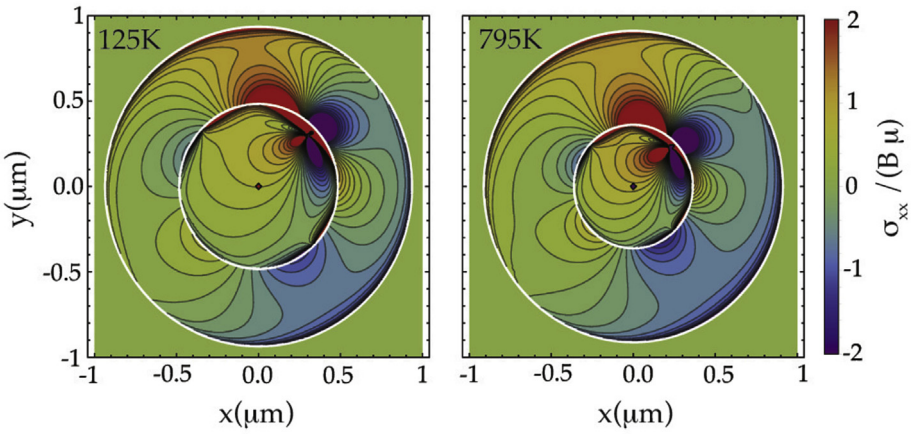

Fig. 15. Global σ_{xx} component of a dislocation that was injected at $(0, 0)$ (marked with a diamond) and moves with uniform speed of $v = 0.9c_t$ in FCC aluminium at 125K and 795K respectively; the case of BCC iron (not represented) is analogous. Note that both the 125K and 795K figures appear analogous. This is intentional, and it highlights that the only difference between the two temperatures is the scaling, modulated by $B\mu$.

Since in the D3P simulation the dislocations are generally moving at an angle with respect to the shock front, and since it is the σ_{xx} component of the stress field that will be responsible for relaxing the shock front, this simplified case is employed here to illustrate the general mechanics of the plastic relaxation of the shock front. For both temperatures, the magnitude of the region responsible for the relaxation of the shock front (in the upper quadrant of both temperatures in Fig. 15) appears to be largely the same; the Doppler-like dynamic magnification of the fields that is a key contributor to the attenuation of the dynamic yield point (Gurrutxaga-Lerma, 2016) is the same in either case.

The crucial difference however lies in the normalisation factor applied to both figures: the magnitude of the stress has been divided by a factor $B\mu$, to highlight that the dynamic stress fields of dislocations are always directly proportional to the shear modulus μ (or a converse elastic constant). Thus, albeit no enhanced contractions or Doppler-like magnifications are observed as a result of an increase in the absolute glide speed of the dislocation, the magnitude of the plastic shielding provided by each dislocation still decreases with increasing temperature simply because the stress of dislocations is transmitted in direct proportion to the shear modulus μ, which does in fact decrease with temperature.

Thus, as the temperature increases, the absolute magnitude of the plastic shielding due to dislocations being generated at the shock front will decrease mainly because the shear modulus of FCC aluminium decreases with temperature. The decrease in plastic shielding effects immediately impacts the attenuation of the dynamic yield point, which becomes weaker at higher temperatures. The decrease in the magnitude of μ for FCC Al over the temperature range tested here is of around 33% for FCC Al; over the same range, the reported experimental increase in the dynamic yield point is around 29.5%. This effect is therefore less related to the drop in the absolute average speeds of dislocations suggested by the Orowan equation, and more to a fundamental change in the elastic constants of the material as a result of a change in the medium's temperature. This is shown in Fig. 16a, which shows the magnitude of the attenuation of the dynamic yield point achieved in the D3P simulations. As can be seen, the magnitude of the yield point achieved in the D3P simulations clearly increases with temperature.

In the case of BCC Fe, the larger amount of dislocations available at the shock front as a result of stronger source activity leads, in turn, to largely the same attenuation of the dynamic yield point over the same temperature range, as is shown in Fig. 16b. Due to computational limitations, the D3P simulations cannot reach the fully relaxed state of the experiments (see section 2); however, the decay observed in Fig. 16a is consistent with the qualitative behaviour observed in experiments and predictions from the MDDP simulations, and as has been argued above, can only be properly explained by a drop in the value of the elastic constants, which is accompanied by a weakening of dislocation interactions.

6. Conclusions

This article has presented the experimental results of the evolution of the dynamic yield point in laser-shocked FCC Al and BCC Fe. The experiments reported here have shown that, in agreement with previous observations, whilst the dynamic yield point of Al increases with temperature, the yield point of Fe remains largely insensitive to temperature. An MDDP model of the said experiments has been developed, through which the importance of dislocation mobility and the Peierls barrier has been highlighted. For Al, the enhanced mobility of edge dislocations relative to screw dislocations appears crucial in producing the required degree of plastic relaxation at the front. Increasing the temperature hinders the motion of the edge components and, crucially, that of screw components even more; ultimately, this results in the increase in the dynamic yield point of Al. For Fe, the mobility of dislocations is more limited to begin with: the general drag coefficients are larger, and the motion of screw components severely limited by much larger Peierls barriers; increasing the temperature does not result in an appreciable change of the yield point because the mobility of dislocations is already compromised to begin with.

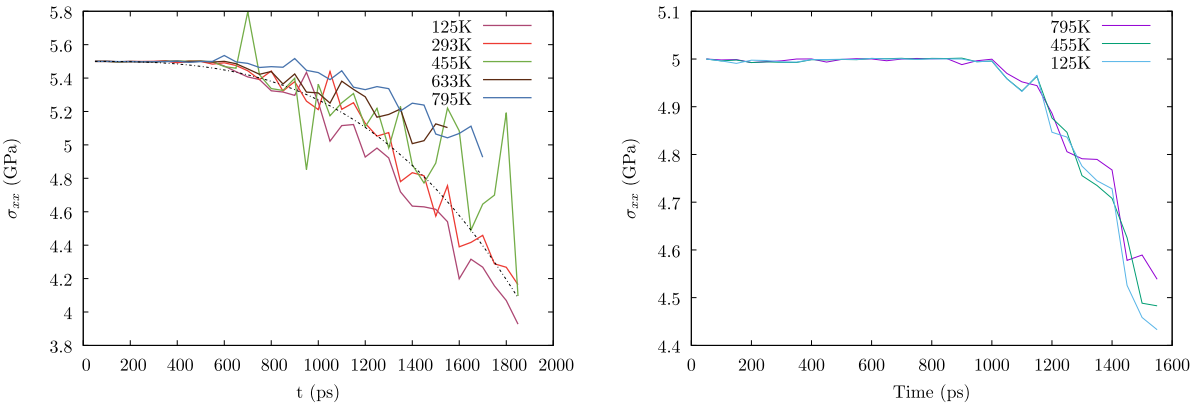

(a) FCC Al. (b) BCC Fe.

Fig. 16. Attenuation of the dynamic yield point at different temperatures for FCC Al and BCC Fe, both shocked at 10^7 s^{-1}.

However, it has been argued that the shock front is not *relaxed* by the speed of dislocations — to wit, plastic yield is not caused by dislocation mobility per se, but by the elastic fields of the dislocations, that negatively interfere with the front itself, shielding it (Gurrutxaga-Lerma et al., 2015b). If plastic yielding is materialised by the elastic fields of dislocations, which interfere with the shock front, how is the relative speed of dislocations relevant to the yielding process? The true fields of dislocations are elastic waves radiated by the moving core. The magnitude of this shielding depends on the speed of the dislocations at the front.

In order to address this point, and owing to the limitations of MDDP yet building on the knowledge extracted from the MDDP simulations, a planar Dynamic Discrete Dislocation Plasticity (D3P) model has been developed to study the attenuation of the elastic precursor in FCC aluminium and BCC iron at different temperatures and for strain rates of the order of 10^7 s^{-1}. Experimental studies reported in this work have shown that at that strain rate, the dynamic yield point of FCC Al increases with temperature, whilst for BCC Fe it remains largely temperature insensitive. From a dislocation dynamics perspective, temperature effects materialise in the magnitude of the elastic constants and density of aluminium, which tend to decrease with increasing temperature; and in the magnitude of the dislocation drag, which is directly proportional to temperature. The D3P analysis has been employed to produce an in-detail study of the causes leading to the dynamic yield point behaviour at the shock front. In this case, it has been shown that the shock front is relaxed by the shielding due to the elastodynamic fields of dislocations, which negatively interfere with the shock front; the magnitude of this shielding has been shown to decay with increasing temperature. Thus, the decrease in the plastic relaxation with increasing temperature is ascribed to effects related to the motion of dislocations at the shock front. It is argued that plastic relaxation occurs as a result of the shielding provided by the fields radiated by moving dislocations, and that the magnitude of the shielding is more strongly affected not by the absolute speed of the dislocations, which has been shown to be fairly close to the transverse speed of sound for all temperatures, but by the drop in the value of the elastic constants, which modulate the magnitude of the shielding fields themselves. Thus, the effect appears to be explained on the grounds that increasing the temperature produces a drop in the value of the elastic constants of the medium, so all dislocation activity becomes weaker; and in terms of the ability of dislocation sources to produce larger numbers to compensate the decrease in the magnitude of the plastic shielding.

Aside from a comprehensive physical explanation of what promotes the thermal hardening of metals at moderate and high strain rates, both the experiments and simulation results presented in this work serve to showcase the fundamental changes that plastic flow experiences as it comes to be governed by dislocations drag. At low strain rates, plastic flow is usually governed by plastic slip, i.e., by the motion of, or the hindering of the motion of, dislocations. Generation mechanisms are secondary at these strain rates. As dislocation motion transcends from being thermally activated to drag-dominated, there is a sudden and well-attested change in the materials strain rate sensitivity (at about $10^3 - 10^4$ s^{-1} for both Fe and Al).

Beyond this point, this work shows that the temperature dependence of the plastic response changes strongly. While thermally activated, plasticity was dominated by an Arrhenius-like law for the mobility of dislocations, so that $\overline{v} \propto e^{-(E(\tau))/(k_B T)}$ (see (Hirth and Lothe, 1982)). Once it becomes drag-controlled (or relativistic), the mobility of dislocations comes to be directly proportional to the temperature itself, via the drag coefficient $d = d_R \cdot T/T_R$. Whilst the Arrhenius form implies greater amount of plastic slip with increasing temperature, the drag-controlled form implies the opposite, a decrease in plastic slip with increasing temperature. The experiments shown in section 2 show thermal hardening, which can only be found in a purely drag-dominated regime.

Furthermore, the simulations show the role relativistic dislocations may play in the plastic response of the material. This is not accounted for in the conventional treatments proposed in the past, usually based on constitutive modelling of the response (see (Kanel et al., 2003; Zaretsky, 1995, 2009, 2010; Zaretsky and Kanel, 2011, 2012, 2013, 2014)). The results

presented here show that the temperature dependence of the limiting speed is of great relevance to explain the experiments. In addition, the simulations highlight the strong correlation that exists between dislocation mobility and dislocation generation mechanisms (in particular, the Frank-Read source mechanism), and highlight that generation is as relevant a source of plastic slip as is dislocation motion. As described above, once the generation and thermal-dependence of the motion are accounted for, the picture that arises is complicated and comprehensive: a clear temperature dependence for Al was observed, which one may explain invoking the temperature dependence of the drag coefficient; however, this temperature dependence is very weak for Fe, which may only be explained by looking at how temperature affects dislocation generation at this strain rate, and at whether or not dislocation motion is fully unhindered.

The insights thus gained may be directly translated to the development and modification of existing constitutive laws for the plastic response of metals. On one hand, the parameters of phenomenological laws such as the Johnson-Cook equation may be tuned via concurrent coupling of the dislocation dynamics model with continuum plasticity-based regions (see (Wallin et al., 2008; Xu et al., 2016)). On the other hand, the results presented here may be directly used to inform the fundamental variable dependence of physically motivated plastic flow rules, such as those based on the Orowan equation (Orowan, 1940) (e.g., the MTS (Follansbee and Kocks, 1988) or Zerilli-Armstrong models (Zerilli and Armstrong, 1987)). In the latter, for instance, given that the temperature response of both metals can only be reproduced by assuming that dislocations move in the drag-controlled and relativistic regimes, any constitutive law attempting to model its response in this regime would have to reflect this, and be modified so that the average dislocation speed be directly proportional to temperature or, otherwise, by adequately modelling the plastic strain rate directly proportional to the temperature.

Acknowledgements

B. Gurrutxaga-Lerma conceived and developed the D3P models, run the simulations and wrote the article. M.A. Shehadeh developed the MDDP models, run the simulations and contributed to the result analysis, discussion and writing of the paper. D. Dini and D.S. Balint interpreted the results and contributed to the writing of the discussions. D.E. Eakins and L. Chen designed and carried out the experiments, and wrote the experimental section. All authors gave their approval for publication.

All data and results are made available upon request by email to the corresponding author or tribology@imperial.ac.uk.

We would like to acknowledge the support received from the EPSRC under D.Dini's Established Career Fellowship grant EP/N025954/1. B. Gurrutxaga-Lerma acknowledges the munificent support of Trinity College Cambridge under his Title A Fellowship. M.A. Shehadeh would like to acknowledge the support from the Research Board and the Faculty of Engineering Dean's office at the American University of Beirut. D. Eakins acknowledges the support of the Institute of Shock Physics at Imperial College London. The authors are also grateful to Los Alamos National Laboratory for experimental support. The authors declare no competing interests.

References

Achenbach, J.D., 1973. Wave Propagation in Elastic Solids, Volume 16 of Applied Mathematics and Mechanics. North-Holland, Oxford, UK.
Argon, A.S., 2008. Strengthening Mechanisms in Crystal Plasticity. Oxford Univ. Press, Oxford, UK.
Armstrong, R.W., Walley, S.M., 2008. High strain rate properties of metals and alloys. Int. Mater. Rev. 53 (3), 105–128.
Balint, D.S., Deshpande, V.S., Needleman, A., Van der Giessen, E., 2005. Discrete dislocation plasticity analysis of crack-tip fields in polycrystalline materials. Philos. Mag. 85 (26–27), 3047–3071.
Balint, D.S., Deshpande, V.S., Needleman, A., Van der Giessen, E., 2006. Size effects in uniaxial deformation of single and polycrystals: a discrete plasticity analysis. Model. Simul. Mater. Sci. Eng. 14, 409–442.
Becker, R., 2004. Effects of crystal plasticity on materials loaded at high pressures and strain rates. Int. J. Plast. 20 (11), 1983–2006.
Benzerga, A.A., 2008. An analysis of exhaustion hardening in micron-scale plasticity. Int. J. Plast. 24, 1128–1157.
Benzerga, A., 2009. Micro-pillar plasticity: 2.5 d mesoscopic simulations. J. Mech. Phys. Solids 57 (9), 1459–1469.
Brown, L.M., 1964. The self-stress of dislocations and the shape of extended nodes. Phil. Mag. 10 (105), 441–466.
Cahn, J.W., 1957. Nucleation on dislocations. Acta Metall. 5 (3), 169–172.
Cai, W., Bulatov, V.V., 2004. Mobility laws in dislocation dynamics simulations. Mater. Sci. Eng. A 387–389, 277–281.
Cho, J., Molinari, J.-F., Anciaux, G., 2016. Mobility law of dislocations with several character angles and temperatures in fcc aluminum. Int. J. Plast. 90, 66–75.
Cleveringa, H.H.M., Van der Giessen, E., Needleman, A., 1999. A discrete dislocation analysis of bending. Int. J. Plast. 15, 837–868.
Clouet, E., 2009. Elastic energy of a straight dislocation and contribution from core tractions. Phil. Mag. 89 (19), 1565–1584.
Cui, Y.N., Lin, P., Liu, Z.L., Zhuang, Z., 2014. Theoretical and numerical investigations of single arm dislocation source controlled plastic flow in fcc micro-pillars. Int. J. Plast. 55, 279–292.
Davoudi, K.M., Nicola, L., Vlassak, J.J., 2014. Bauschinger effect in thin metal films: discrete dislocation dynamics study. J. Appl. Phys. 115(1) (013507).
De Rességuier, T., Lescoute, E., Loison, D., 2012. Influence of elevated temperature on the wave propagation and spallation in laser shock-loaded iron. Phys. Rev. B 86 (21), 214102.
Dever, D.J., 1972. Temperature dependence of the elastic constants in α-iron single crystals: relationship to spin order and diffusion anomalies. J. Appl. Phys. 43 (8), 3293–3301.
Domain, C., Monnet, G., 2005. Simulation of screw dislocation motion in iron by molecular dynamics simulations. Phys. Rev. Lett. 95, 215506.
Follansbee, P.S., Kocks, U.F., 1988. A constitutive description of the deformation of copper based on the use of the mechanical threshold stress as an internal state variable. Acta Metall. 36 (1), 81–93.
Foreman, A.J.E., 1967. The bowing of a dislocation segment. Phil. Mag. 15, 1011–1021.
Franciosi, P., Le, L.T., Monnet, G., Kahloun, C., Chavanne, M.-H., 2015. Investigation of slip system activity in iron at room temperature by sem and afm in-situ tensile and compression tests of iron single crystals. Int. J. Plast. 65, 226–249.
Garcia-Gonzalez, D., Zaera, R., Arias, A., 2017. A hyperelastic-thermoviscoplastic constitutive model for semi-crystalline polymers: application to peek under dynamic loading conditions. Int. J. Plast. 88, 27–52.
Gilbert, M.R., Schuck, P., Sadigh, B., Marian, J., 2013. Free energy generalization of the peierls potential in iron. Phys. Rev. Lett. 111 (9), 095502.

Gillis, P.P., Gilman, J.J., Taylor, J.W., 1969. Stress dependences of dislocation velocities. Phil. Mag. 20 (164), 279–289.
Groh, S., Marin, E.B., Horstemeyer, M.F., Zbib, H.M., 2009. Multiscale modeling of the plasticity in an aluminum single crystal. Int. J. Plast. 25 (8), 1456–1473.
Gurrutxaga-Lerma, B., 2016. The role of the mobility law of dislocations in the plastic response of shock loaded pure metals. Model. Simul. Mater. Sci. Eng. 24 (6), 065006.
Gurrutxaga-Lerma, B., 2017. How strong is the temperature increase due to a moving dislocation? Int. J. Solids Struct. 108, 263–274.
Gurrutxaga-Lerma, B., Balint, D.S., Dini, D., Eakins, D.E., Sutton, A.P., 2013. A dynamic discrete dislocation plasticity method for the simulation of plastic relaxation under shock loading. Proc. Roy. Soc. A 469, 20130141.
Gurrutxaga-Lerma, B., Balint, D.S., Dini, D., Eakins, D.E., Sutton, A.P., 2014. Dynamic Discrete Dislocation Plasticity, Volume 47 of Advances in Applied Mechanics, Chapter 2. Elsevier.
Gurrutxaga-Lerma, B., Balint, D.S., Dini, D., Sutton, A.P., 2015. The mechanisms governing the activation of dislocation sources in aluminum at different strain rates. J. Mech. Phys. Solids 84, 273–292.
Gurrutxaga-Lerma, B., Balint, D.S., Dini, D., Eakins, D.E., Sutton, A.P., 2015. Attenuation of the dynamic yield point of shocked aluminum using elastodynamic simulations of dislocation dynamics. Phys. Rev. Lett. 114, 174301.
Gurrutxaga-Lerma, B., Balint, D.S., Dini, D., Eakins, D.E., Sutton, A.P., 2015. The role of homogeneous nucleation in planar dynamic discrete dislocation plasticity. J. Appl. Mech. 82 (071008).
Hirth, J.P., Lothe, J., 1982. Theory of Dislocations, second ed. John Wiley & Sons, New York.
Ho, P.S., Ruoff, A.L., 1969. Pressure dependence of the elastic constants for aluminum from 77 to 300k. J. Appl. Phys. 40 (8), 3151–3156.
Hornbogen, E., 1962. Shock-induced dislocations. Acta Metall. 10 (10), 978–980.
Hull, D., Bacon, D.J., 2011. Introduction to Dislocations, fifth ed. Butterworth-Heinemann, Oxford, UK.
Hunter, A., Preston, D.L., 2015. Analytic model of the remobilization of pinned glide dislocations from quasi-static to high strain rates. Int. J. Plast. 70, 1–29.
Imura, T., Noda, K., Matsui, H., Saka, H., Kimura, H., 1985. Direct measurement of mobility of dislocations in high-purity molybdenum. In: Suzuki, H., Nonomiya, T., Sumino, K., Takeuchi, S. (Eds.), Dislocations in Solids. Yamada Science Foundation, University of Tokyo Press, Tokyo, JP, pp. 287–290.
Itakura, Mitsuhiro, Kaburaki, Hideo, Yamaguchi, Masatake, 2012. First-principles study on the mobility of screw dislocations in bcc iron. Acta Mater. 60 (9), 3698–3710.
Kanel, G.I., Razorenov, S.V., Zaretsky, E.B., Herrman, B., Meyer, L., 2003. Thermal “softening” and “hardening” of titanium and its alloy at high strain rates of shock-wave deforming. Phys. Solid State 45 (4), 656–661.
Kattoura, M., Shehadeh, M.A., 2014. On the ultra-high-strain rate shock deformation in copper single crystals: multiscale dislocation dynamics simulations. Philos. Mag. Lett. 94 (7), 415–423.
Khan, S.M.A., Zbib, H.M., Hughes, D.A., 2004. Modeling planar dislocation boundaries using multi-scale dislocation dynamics plasticity. Int. J. Plast. 20 (6), 1059–1092.
Kubin, L.P., 2013. Dislocations, Mesoscale Simulations and Plastic Flow. volume 5 of Oxford Series on Materials Modelling. Oxford Univ. Press, Oxford, UK.
Lawley, A., Gaigher, H.L., 1964. Deformation structures in zone-melted molybdenum. Philos. Mag. 10 (103), 15–33.
Levy, M., Bass, H., Stern, R., 2000. Handbook of Elastic Properties of Solids, Liquids, and Gases, Four-volume Set, vol. 2. Academic Press.
Li, J., Wang, C.-Z., Chang, J.-P., Cai, W., Bulatov, V.V., Ho, K.-M., Yip, S., 2004. Core energy and peierls stress of a screw dislocation in bcc molybdenum: a periodic-cell tight-binding study. Phys. Rev. B 70 (10), 104113.
Lim, Hojun, Hale, L.M., Zimmerman, J.A., Battaile, C.C., Weinberger, C.R., 2015. A multi-scale model of dislocation plasticity in α-fe: incorporating temperature, strain rate and non-schmid effects. Int. J. Plast. 73, 100–118.
Markenscoff, X., Clifton, R.J., 1981. The nonuniformly moving edge dislocation. J. Mech. Phys. Solids 29 (2), 253–262.
Meyers, M.A., 1994. Dynamic Behavior of Materials. John Wiley, Hoboken, NJ.
Meyers, M.A., Jarmakani, H., Bringa, E.M., Remington, B.A., 2009. Dislocations in shock compression and release. In: Hirth, J.P., Kubin, L.P. (Eds.), Dislocations in Solids, vol. 15. North-Holland, pp. 94–197 chapter 89.
Monnet, G., Terentyev, D., 2009. Structure and mobility of the edge dislocation in bcc iron studied by molecular dynamics. Acta Mater. 57 (5), 1416–1426.
Nabarro, F.R.N., 1967. Theory of Crystal Dislocations. Oxford Univ. Press, Oxford, UK.
Nicola, L., Van der Giessen, E., Needleman, A., 2001. 2d dislocation dynamics in thin metal layers. Mater. Sci. Eng. A 309, 274–277.
Nicola, L., Van der Giessen, E., Needleman, A., 2003. Discrete dislocation analysis of size effects in thin films. J. Appl. Phys. 93, 5920.
Olmsted, D.L., Hector, L.G., Curtin, W.A., Clifton, R.J., 2005. Atomistic simulations of dislocation mobility in Al, Ni and Al/Mg alloys. Model. Simul. Mater. Sci. Eng. 13, 371–388.
Orowan, E., 1940. Problems of plastic gliding. Proc. Phys. Soc. 52, 8–22.
Queyreau, S., Marian, J., Gilbert, M.R., Wirth, B.D., 2011. Edge dislocation mobilities in bcc fe obtained by molecular dynamics. Phys. Rev. B 84 (064106).
Reed-Hill, R.E., Abbaschian, R., Abaschian, L., 2009. Physical Metallurgy Principles, fourth ed. Cengage Learning, Stamford, CT.
Rice, J.R., 1987. Tensile crack tip fields in elastic-ideally plastic crystals. Mech. Mater. 6, 317–335.
Rohde, R.W., 1969. Dynamic yield behavior of shock-loaded iron from 76 to 573k. Acta Metall. 17, 353–363.
Salehinia, I., Bahr, D.F., 2014. Crystal orientation effect on dislocation nucleation and multiplication in fcc single crystal under uniaxial loading. Int. J. Plast. 52, 133–146.
Shehadeh, M.A., 2012. Multiscale dislocation dynamics simulations of shock-induced plasticity in small volumes. Phil. Mag. 92 (10), 1173–1197.
Shehadeh, M.A., Zbib, H.M., 2016. On the homogeneous nucleation and propagation of dislocations under shock compression. Philos. Mag. 96 (26), 2752–2778.
Shehadeh, M.A., Zbib, H.M., Diaz de la Rubia, T., 2005. Multiscale dislocation dynamics simulations of shock compression in copper single crystal. Int. J. Plast. 21, 2369–2390.
Shehadeh, M.A., Bringa, E.M., Zbib, H.M., McNaney, J.M., Remington, B.A., 2006. Simulation of shock-induced plasticity including homogeneous and heterogenous dislocation nucleations. Appl. Phys. Lett. 89, 171818.
Shishvan, S.S., Van der Giessen, E., 2010. Distribution of dislocation source length and the size dependent yield strength in freestanding thin films. J. Mech. Phys. Solids 58 (5), 678–685.
Tschopp, M.A., McDowell, D.L., 2008. Influence of single crystal orientation on homogeneous dislocation nucleation under uniaxial loading. J. Mech. Phys. Solids 56, 1806–1830.
Urabe, N., Weertman, J., 1975. Dislocation mobility in potassium and iron single crystals. Mater. Sci. Eng. 18 (1), 41–49.
Van der Giessen, E., Needleman, A., 1995. Discrete dislocation plasticity: a simple planar model. Model. Simul. Mater. Sci. Eng. 3 (5), 689–735.
Wallin, M., Curtin, W.A., Ristinmaa, M., Needleman, A., 2008. Multi-scale plasticity modeling: coupled discrete dislocation and continuum crystal plasticity. J. Mech. Phys. Solids 56 (11), 3167–3180.
Wang, Z.Q., Beyerlein, I.J., 2011. An atomistically-informed dislocation dynamics model for the plastic anisotropy and tension–compression asymmetry of bcc metals. Int. J. Plast. 27 (10), 1471–1484.
Xu, Y., Balint, D.S., Dini, D., 2016. A method of coupling discrete dislocation plasticity to the crystal plasticity finite element method. Model. Simul. Mater. Sci. Eng. 24 (4), 045007.
Yanilkin, A.V., Krasnikov, V.S., Kuksin, A., Mayer, A.E., 2014. Dynamics and kinetics of dislocations in al and al–cu alloy under dynamic loading. Int. J. Plast. 55, 94–107.
Zaretsky, E., 1995. Dislocation multiplication behind the shock front. J. Appl. Phys. 78 (6), 3740–3747.
Zaretsky, E.B., 2009. Shock response of iron between 143 and 1275 k. J. Appl. Phys. 106 (2), 023510.
Zaretsky, E.B., 2010. Impact response of cobalt over the 300-1400k temperature range. J. Appl. Phys. 108 (8).

Zaretsky, E.B., Kanel, G.I., 2011. Plastic flow in shock-loaded silver at strain rates from 10^4 s^{-1} to 10^7 s^{-1} and temperatures from 296k to 1233k. J. Appl. Phys. 110 (7).
Zaretsky, E.B., Kanel, G.I., 2012. Effect of temperature, strain, and strain rate on the flow stress of aluminum under shock-wave compression. J. Appl. Phys. 112 (7), 073504.
Zaretsky, E.B., Kanel, G.I., 2013. Response of copper to shock-wave loading at temperatures up to the melting point. J. Appl. Phys. 114 (8).
Zaretsky, E.B., Kanel, G.I., 2014. Tantalum and vanadium response to shock-wave loading at normal and elevated temperatures. non-monotonous decay of the elastic wave in vanadium. J. Appl. Phys. 115 (24), 243502.
Zbib, H.M., Diaz de la Rubia, T., 2002. A multiscale model of plasticity. Int. J. Plast. 18 (9), 1133–1163.
Zbib, H.M., Shehadeh, M., Khan, S.M.A., Karami, G., 2003. Multiscale dislocation dynamics plasticity. Int. J. Multiscale Comput. Eng. 1 (1).
Zerilli, F.J., Armstrong, R.W., 1987. Dislocation-mechanics-based constitutive relations for material dynamics calculations. J. Appl. Phys. 5, 1816–1825.
Zhu, Y., Wang, H., Zhu, X., Xiang, Y., 2014. A continuum model for dislocation dynamics incorporating frank–read sources and hall–petch relation in two dimensions. Int. J. Plast. 60, 19–39.